THE ASTROPHYSICAL JOURNAL SUPPLEMENT SERIES, 129:399–420, 2000 July

AN *IUE* ATLAS OF PRE–MAIN-SEQUENCE STARS. I. CO-ADDED FINAL ARCHIVE SPECTRA FROM THE SWP CAMERA

JEFF A. VALENTI[1]
Space Telescope Science Institute, 3700 San Martin Drive, Baltimore, MD 21218; valenti@stsci.edu
AND
CHRISTOPHER M. JOHNS-KRULL[2] AND JEFFREY L. LINSKY
JILA, University of Colorado and NIST, Boulder, CO 80309-0440; cmj@ssl.berkeley.edu, jlinsky@jila.colorado.edu
Received 1999 November 21; accepted 2000 February 25

ABSTRACT

We have identified 50 T Tauri stars (TTS) and 74 Herbig Ae/Be (HAEBE) stars observed in the *IUE* short-wavelength bandpass (1150–1980 Å). Each low-resolution ($R \sim 6$ Å) spectrum was visually inspected for source contamination and data quality, and then all good spectra were combined to form a single time-averaged spectrum for each star. Use of *IUE* Final Archive spectra processed with NEWSIPS reduces fixed pattern noise in individual spectra, allowing significant signal-to-noise ratio gains in our co-added spectra. For the TTS observed by *IUE*, we measured fluxes and uncertainties for 17 spectral features, including two continuum windows and four fluoresced H_2 complexes. Thirteen of the 32 accreting TTS observed by *IUE* have detectable H_2 emission, which until now had been reported only for T Tau. Using an empirical correlation between H_2 and C IV line flux, we show that lack of sensitivity can account for practically all nondetections, suggesting that H_2 fluorescence may be intrinsically strong in all accreting TTS systems. Comparison of *IUE* and GHRS spectra of T Tau show extended emission primarily, but not exclusively, in lines of H_2. We also fit reddened main-sequence templates to 72 HAEBE stars, determining extinction and checking spectral types. Several of the HAEBE stars could not be fitted well or yielded implausibly low extinctions, suggesting the presence of a minority emission component hotter than the stellar photosphere, perhaps caused by white dwarf companions or heating in accretion shocks. We identified broad wavelength intervals in the far-UV that contain circumstellar absorption features ubiquitous in B5–A4 HAEBE stars, declining in prominence for earlier spectral types, perhaps caused by increasing ionization of metal resonance lines. For 61 HAEBE stars, we measured or set upper limits on a depth index that characterizes the strength of circumstellar absorption and compared this depth index with published IR properties.

Subject headings: accretion, accretion disks — atlases — stars: pre–main-sequence — ultraviolet: stars

On-line materials: extended table

1. INTRODUCTION

On 1996 September 27, the *International Ultraviolet Explorer* (*IUE*) satellite ceased real-time operations. Over the course of its 18 yr lifetime, *IUE* acquired several thousand spectra of pre–main-sequence (PMS) stars, many of which have never been published. A few higher quality spectra have been obtained with ultraviolet (UV) spectrographs on the *Hubble Space Telescope* (*HST*), but halfway through its nominal lifetime, *HST* has reobserved only about 10% of the PMS stars studied by *IUE*. If this trend continues, *IUE* archival spectra of PMS stars will remain an important resource for many years.

Older *IUE* analyses generally interpret UV emission exclusively in terms of a deep chromosphere (e.g., Giampapa et al. 1981; Herbig & Goodrich 1986), whereas now accretion must also be considered (e.g., Simon, Vrba, & Herbst 1990; Goméz de Castro & Lamzin 1999). The *IUE* short-wavelength (SWP) camera covered the wavelength range 1150–1980 Å, which includes several interesting emission lines that might diagnose accretion, most notably lines of C IV and Si IV. Therefore, it is useful to have a uniform set of SWP spectra and emission-line fluxes for all PMS stars observed with *IUE*.

Another motivation for this project is the enhanced quality and uniformity of *IUE* Final Archive spectra (Nichols & Linsky 1996). Most low-dispersion ($R \sim 6$ Å) spectra have been uniformly reprocessed with the NEWSIPS software (described in detail by Nichols et al. 1994). Reprocessing often yields a significant improvement in signal-to-noise ratios (S/N), especially for weak, high-background, or co-added spectra. Substantial improvements have also been realized in wavelength and photometric calibrations. Such improvements have permitted new identification of H_2 fluorescent emission in 12 PMS stars, as described below. This discovery illustrates how a large sample of UV spectra can facilitate the study of PMS stars and their environments.

Accretion disks are intimately related to the star formation process. Angular momentum conservation during the initial contraction of a protostellar cloud eventually leads to a central PMS star surrounded by a disk. As angular momentum is transported outward through the disk, material must move from the disk either onto the star or into a wind. The current view of star formation suggests that a substantial portion of a star's final mass is accreted

[1] Formerly at JILA, University of Colorado, Boulder, CO 80309-0440.
[2] Now at Space Sciences Laboratory, University of California, Berkeley, Berkeley, CA 94720.

through such a disk (Shu, Adams, & Lizano 1987). Disk material impacting the star is shock heated, producing UV radiation, which makes *IUE* observations potentially diagnostic of the accretion process on PMS stars.

Very few high-mass PMS stars are available for study, but a large number of low- to intermediate-mass PMS stars have been catalogued. These PMS stars generally are divided into the low-mass ($M \lesssim 2.5\ M_\odot$) T Tauri stars (TTS) and the intermediate-mass ($1.5\ M_\odot \lesssim M \lesssim 10\ M_\odot$) Herbig Ae/Be (HAEBE) stars, where the mass overlap in these definitions is age dependent. Below, we follow tradition and retain this class distinction, but our motivation for presenting a combined catalog is to encourage the search for physical processes common to all PMS stars, despite very obvious observational distinctions. Diagnostic measurements possible only in one class of PMS stars may nonetheless yield insight relevant to the other classes.

Properties of TTS have been reviewed by several authors (e.g., Bertout 1989; Appenzeller & Mundt 1989; Basri & Bertout 1993), and their status as low-mass PMS stars is well established. TTS were originally divided into two groups based solely on Hα equivalent width. Stars with strong Hα emission were called classical TTS (CTTS), while the rest were called weak TTS (WTTS) (see Bertout 1989, for example). Several lines of investigation have shown that CTTS are surrounded by active accretion disks that interact with the central star to produce many of the spectral peculiarities characteristic of CTTS (e.g., Bertout 1989). In the literature, the term CTTS has come to be synonymous for a TTS surrounded by an accretion disk. FU Ori stars (see review by Hartmann & Kenyon 1996) are extreme CTTS, in which an instability leads to mass accretion enhanced by a factor of $\sim 10^3$ relative to typical CTTS. FU Ori outbursts appear to last ~ 100 yr, during which time the disk outshines the star by a factor of 100–1000.

While many WTTS lack close circumstellar accretion disks, several intrinsically bright, generally hotter, WTTS do possess close circumstellar disks and are actively accreting at rates comparable to CTTS (examples include SU Aur and Sz 68). Hα equivalent width is low only because the stellar continuum is bright, not because Hα emission-line flux is low. Walter (1987) has proposed the term naked TTS (NTTS) to refer to diskless T Tauri stars and, hence, remove the ambiguity of the term WTTS with regard to the presence of a disk. We adopt this more physical definition and use NTTS wherever possible, using CTTS to refer to any TTS known to be accreting from a disk, regardless of Hα equivalent width.

Basic properties of HAEBE stars have been reviewed recently by Waters & Waelkens (1998). Location in the H-R diagram confirms their PMS status. Hillenbrand et al. (1992) made one of the first attempts to understand HAEBE stars in a relatively global context by analyzing spectral energy distributions for a large sample of stars. They categorize HAEBE stars into three groups, similar to IR spectral classes for TTS: Group II with flat or rising IR energy distributions, consistent with a circumstellar disk plus residual infall envelope; Group I with IR excesses characteristic of a disk; and Group III with no significant IR excess relative to older stars with no circumstellar material. Soon after publication, this paper came under attack as various investigators failed to find evidence confirming the presence of accretion disks (e.g., Hartmann, Kenyon, & Calvet 1993; Böhm & Catala 1994). Recently, disklike structures have been imaged around the HAEBE star AB Aur (Grady et al. 1999b), but even so the general character of circumstellar material around HAEBE stars is still unclear (Waters & Waelkens 1998).

Given the confusion as to whether or not extended circumstellar material around HAEBE stars is in a disk, it is useful to search for direct evidence of material reaching the stellar surface. Accretion onto cool TTS produces shocked material hot enough to produce a detectable continuum excess at blue and UV wavelengths. Spectral line depths become weaker, relative to the enhanced continuum. Similar veiling of optical lines seems not to be present in HAEBE stars (Böhm & Catala 1993; Ghandour et al. 1994), with only a few exceptions, which are restricted to cooler HAEBE stars (Blondel & Tjin a Djie 1994). On the other hand, in TTS, accretion heats material to 10^4 K, which is similar to photospheric temperatures of HAEBE stars. Little is known about how difficult is would be to distinguish accretion and photospheric emission in optical spectra of HAEBE stars. Transient, redshifted absorption features have been observed in a number of HAEBE stars, but these features generally have been interpreted in terms of evaporating comets and phenomena such as can be observed in β Pic (e.g., Grady et al. 1997; De Winter et al. 1999) rather than as accretion from a massive disk.

There is one existing atlas of TTS spectra obtained with *IUE*. Goméz de Castro & Franqueira (1997a) compiled an atlas of pre-final archive low-dispersion (short- and long-wavelength) *IUE* spectra of all TTS observed through 1992 November. In addition to plotting average spectra for each star, Goméz de Castro & Franqueira (1997a) also present for each star a limited number of line fluxes without associated uncertainties. Malfait, Bogaert, & Waelkens (1998) used *IUE* and other data to study the spectral energy distributions of 45 HAEBE stars, but we are not aware of any existing spectroscopic atlases of HAEBE stars observed with *IUE*. Imhoff & Appenzeller (1987) list all PMS sources observed by *IUE* at the time of the review but show only representative spectra. As described above, completion of the *IUE* Final Archive offered a natural starting point for the compilation of a new atlas of SWP spectra of all PMS stars observed by *IUE*.

As we were completing this atlas, we received a draft of Huélamo, Franqueira, & Goméz de Castro (2000) describing their plans to eventually make available a compendium of line fluxes for T Tauri stars based on *IUE* Newly Extracted Spectra (INES). INES is a separate processing of the *IUE* data intended to overcome some potential disadvantages in NEWSIPS (Rodríguez-Pascual et al. 1999). Fortunately, Huélamo et al. (2000) have made detailed comparison of the NEWSIPS and INES data for TTS and find that results generally agree to within the errors reported by the two processing packages.

In § 2, we describe our sample selection criteria and the procedure we used to retrieve and combine *IUE* spectra. In § 3, we present the atlas of co-added spectra, discuss spectral line identifications, present emission-line fluxes for TTS, and characterize extinction and circumstellar absorption toward HAEBE stars. Finally, in § 4 we discuss a few immediate implications of these new measurements, highlighting future possibilities. In a companion paper (Johns-Krull, Valenti, & Linsky 2000, hereafter Paper II), we use the line fluxes presented here to explore the relative importance of (magnetic) activity and accretion to UV emission from TTS.

2. CONSTRUCTING THE ATLAS

2.1. *Defining the Sample*

In constructing this atlas, we attempted to identify every *IUE* SWP exposure with a suspected PMS star in the field of view. Although the *IUE* Merged Log lists source names and object classes, nonuniformities in these data make them unreliable as selection criteria. Instead, we compared the coordinates of *IUE* exposures with positions of known PMS stars, initially selecting all *IUE* observations within 2′ of PMS stars listed in Herbig & Bell (1988), Jones & Walker (1988), Feigelson et al. (1993), Thé, de Winter, & Pérez (1994), or Walter et al. (1994). We identified an additional 10 PMS stars listed in SIMBAD (object types pr*, TT*, Or*, or FU*), but not in the catalogs cited above, that were potentially observed by *IUE*.

We compared source positions with *IUE* pointings contained in an interactive data language (IDL) database version of the *IUE* Merged Log that included all observations through 1996 April 6. Whenever available, the Merged Log right ascensions and declinations were taken from the homogeneous NEWSIPS reprocessing rather than using the original coordinates supplied by the observer. Despite our efforts, it is still likely that we have missed a few PMS stars that were observed with the *IUE* SWP camera.

Table 1 lists the 161 sources identified as just outlined. We assign each source an identification number between 1 and 161 to simplify cross-references within this series of papers, but in general standard nomenclature should be used to refer to individual objects. Column (2) of Table 1 lists the Herbig & Bell (1988) catalog number, if applicable. Alternate source names are given in columns (3) and (4) with catalog precedence as described in the table note. Column (5) gives spectral types selected preferentially from Herbig & Bell (1988), Thé et al. (1994), and then the other source material used in defining the sample. We present these spectral types without comment as to their veracity. Column (6) classifies each source as a Herbig Ae/Be (HAEBE), classical T Tauri (CTTS), naked T Tauri (NTTS), T Tauri of unknown ilk (TTS), or FU Ori (FUORI). In some cases, these classifications are subjective and hence subject to change. Column (7) gives the number of spectra ultimately used to produce our atlas spectrum. Sources with no usable spectra are retained to flag the existence of data. The final two columns list right ascension and declination (equinox 1950) taken from the source catalogs used to define the sample.

2.2. *Combining the Spectra*

Our search of the *IUE* Merged Log yielded camera sequence numbers (e.g., SWP53049) for 707 exposures of 161 PMS sources. Some images contain two adjacent spectra, which were obtained by exposing once with the source on the large aperture and once with it on the small aperture prior to a single read of the detector. As a result, the 707 images actually contain 761 spectra. Using the NASA Data Archive and Distribution Service (NDADS), we were able to retrieve data for 644 images containing 695 spectra (a 91% success rate). The remaining 66 spectra in 63 images were not available in the Final Archive, presumably indicating severe data quality problems in these images. In case the archive calibration or completeness does change, we note that all spectra were retrieved in late October 1996.

Table 2 gives the camera sequence numbers of all SWP images deemed interesting after examining the *IUE* Merged Log. The "ID" numbers in the range 1–161 are source identification numbers corresponding to the first column of Table 1. The five-digit numbers listed by each source specification are image sequence numbers for the SWP camera. For example, source 18 (DK Tau) was observed only in image SWP49748. No spectra of PMS stars were obtained with the SWR camera. Many of the image sequence numbers are also followed by superscripted quality indicators, which are detailed in the table notes. Some notations give information about spectra that were *not* used in constructing the combined spectra, while other notations provide additional information about spectra that *were* used to construct the final spectra.

An interactive procedure was used to assess whether each individual spectrum warranted inclusion in the final weighted mean spectrum. Individual spectra were overplotted in color on a plot of the mean spectrum. For sources with many observations, individual spectra were examined successively in groups of six. Spectra were excluded from the mean for a variety of reasons, which are recorded in the notes for Table 2. Common reasons for rejecting spectra included no apparent signal, a hopelessly noisy spectrum, anomalously low flux, questionable spectral features, a preponderance of bad pixels ($>10\%$ with ν flags ≤ -16, indicating a wide range of serious data problems), or indications of trouble noted in the NEWSIPS header. Table 3 lists the FITS header fields that were inspected and the nominal acceptance criteria we adopted from Chapter 13 of Nichols et al. (1994). Occasionally, we retained a spectrum that failed one or more acceptance test, if the spectrum appeared better than all other spectra of the source. Such instances are noted in Table 2.

Good spectra for each source were combined into a weighted mean spectrum, constructing weights from the flux uncertainties ("SIGMA" vector) in each MXLO file. Pixels in individual spectra with data quality flags ("QUALITY" vector) less than -15 were not used in the combining process, unless the data quality for a particular pixel was worse than this threshold for all constituent spectra. Using a weighted mean maximizes the S/N ratio in the combined spectrum, if the actual flux level of the source is constant. For variable sources (see § 2.3), however, this weighting scheme favors fainter spectra, which have lower flux uncertainties, because Poisson fluctuations in measured "flux numbers" are scaled by a smaller calibration factor. For variable sources, better S/N ratios in the combined spectrum could perhaps be achieved by weighting according to the S/N ratio in each individual spectrum, but we did not attempt this procedure. We determined the formal uncertainty in the combined spectrum by normal propagation of errors so that the reciprocal variance of a pixel in the combined spectrum is the sum of the reciprocal variances for that pixel in each individual spectrum. We also constructed a mean data quality vector for each source, again using flux uncertainties to construct weights.

There were small variations in the wavelength scale ("WAVE") for individual spectra, but the corresponding shift was always less than 0.05 pixel. We combined spectra using uninterpolated pixels since the spurious broadening introduced by ignoring wavelength shifts is at most 1% of the line width. The final wavelength scale for each source is simply the unweighted mean of the wavelength scales for the constituent spectra and is very similar for all sources.

TABLE 1

PRE–MAIN-SEQUENCE STARS OBSERVED BY *IUE* WITH SWP CAMERA

ID[a] (1)	HBC[b] (2)	Name[c] (3)	Alternate Name[c] (4)	Type[d] (5)	Category (6)	N[e] (7)	α (1950) (8)	δ (1950) (9)
1	329	VX Cas	...	A0, 3eV	HAEBE	0	00 28 40.44	+61 42 17
2	330	V594 Cas	MWC 419	B:eq	HAEBE	2	00 40 21.94	+61 38 15
3	10	LkHα 264	...	K5 V (Li)	CTTS	2	02 53 46.92	+19 53 33
4	345	HH 12/107	SSS 107	M0:	CTTS	1	03 25 52.5	+31 07 46
5	349	XY Per w	HD 275877	A5:eα	HAEBE	0	03 46 17.20	+38 49 49
6	...	BD +21 584	SAO 76428	F8	NTTS	1	04 01 31	+21 47 56.0
7	367	V773 Tau	HD 283447	K3 V (Li)	NTTS	0	04 11 07.29	+28 04 41
8	29	V410 Tau	BD +28 637	K3 V (Li)	NTTS	2	04 15 24.83	+28 20 01
9	32	BP Tau	MHα 259–7	K7 V (Li)	CTTS	14	04 16 08.61	+28 59 15
10......	33	DE Tau	MHα 259–8	M2:V (Li)	CTTS	2	04 18 49.84	+27 48 05
11......	34	RY Tau	BD +28 645	K1 IV, V (Li)	CTTS	13	04 18 50.85	+28 19 35
12......	380	HD 283572	BD +27 657	G5 IV (Li)	NTTS	3	04 18 52.52	+28 11 06
13......	35	T Tau	BD +19 706	K0 IV, V (Li)	CTTS	4	04 19 04.21	+19 25 05
14......	36	DF Tau	MHα 259–11	M0, 1 V (Li)	CTTS	3	04 23 59.63	+25 35 41
15......	37	DG Tau	MHα 259–10	M?	CTTS	2	04 24 01.01	+25 59 35
16......	388	NTTS 042417+1744	...	K1 (Li)	NTTS	0	04 24 17.2	+17 44 03
17......	43	UX Tau A	BD +17 736	K2 V (Li)	NTTS	1	04 27 09.96	+18 07 21
18......	45	DK Tau	MHα 259–12	K7 V (Li)	CTTS	1	04 27 40.48	+25 54 59
19......	393	L1551/IRS 5	...	K2 III:	CTTS	1	04 28 40.22	+18 01 41
20......	49	HL Tau	Haro 6–14	K7, M2?	CTTS	0	04 28 44.42	+18 07 36
21......	405	V830 Tau	WK2	K7, M0 V (Li)	NTTS	0	04 30 08.26	+24 27 26
22......	56	GI Tau	Haro 6–21	K6 V (Li)	CTTS	1	04 30 32.33	+24 15 03
23......	57	GK Tau	Haro 6–22	K7 V (Li)	CTTS	0	04 30 32.76	+24 14 52
24......	58	DL Tau	MHα 259–13	K7V (Li)	CTTS	1	04 30 36.02	+25 14 24
25......	63	AA Tau	MHα 259–17	K7 V (Li)	CTTS	1	04 31 53.45	+24 22 44
26......	...	HD 283817	BD +24 676	A3e/G0e	HAEBE	0	04 37 30.47	+24 20 45.3
27......	74	DR Tau	MHα 257–8	...	CTTS	11	04 44 13.20	+16 53 23
28......	75	DS Tau	MHα 259–2	K5 V (Li)	CTTS	1	04 44 39.07	+29 19 56
29......	77	GM Aur	MHα 259–1	K3 V (Li)	CTTS	2	04 51 59.76	+30 17 14
30......	426	LkCa 19	NTTS 045226+3013	K0 V (Li)	NTTS	1	04 52 25.90	+30 13 10
31......	78	AB Aur	HD 31293	B9, A0e+sh	HAEBE	94	04 52 34.24	+30 28 21
32......	79	SU Aur	HD 282624	G2 III (Li)	CTTS	7	04 52 47.84	+30 29 19
33......	...	HD 31648	MWC 480	A2/3ep+sh	HAEBE	4	04 55 35.54	+29 46 06.3
34......	430	UX Ori	BD −4 1029	A3e III	HAEBE	11	05 02 00.62	−03 51 19
35......	80	RW Aur A	BD +30 792	K1:	CTTS	8	05 04 37.69	+30 20 13
36......	...	V346 Ori	HD 287841	A5 III:e	HAEBE	1	05 22 07.9	+01 40 57
37......	...	HD 35929	BD −08 1128	A5e	HAEBE	4	05 25 18.74	−08 22 04.4
38......	85	GW Ori	BD +11 819	G5 (Li)	CTTS	3	05 26 20.78	+11 49 52
39......	...	HD 36112	MWC 758	A3e	HAEBE	0	05 27 22.45	+25 17 42.7
40......	94	HK Ori	MWC 497	Aep	HAEBE	2	05 28 40.08	+12 07 00
41......	436	RY Ori	...	F8:pe (Li)	CTTS	0	05 29 39.57	−02 51 55
42......	443	HD 245059	λ Ori X–1	K3 V: (Li)	NTTS	1	05 31 49.26	+10 05 10
43......	113	V1044 Ori	Parenago 1404	G5 IV, V (Li)	CTTS	0	05 31 49.28	−05 38 43
44......	...	V372 Ori	HD 36917	A0 V	HAEBE	1	05 32 19.70	−05 36 10.7
45......	451	HD 245185	BD +9 880	A5eα	HAEBE	4	05 32 24.08	+09 59 57
46......	122	KM Ori	Parenago 1659	K1 (Li)	NTTS	0	05 32 28.48	−05 25 07
47......	126	LL Ori	Parenago 1746	K2, 3 (Li)	HAEBE	2	05 32 38.18	−05 27 13
48......	129	V356 Ori	Parenago 1773	K3	HAEBE	1	05 32 41.68	−05 31 53
49......	...	LP Ori	HD 36982	B1.5 V	HAEBE	1	05 32 42.47	−05 29 47.1
50......	458	MT Ori	Parenago 1910	K3, 4 (Li)	HAEBE	18	05 32 50.42	−05 24 38
51......	...	V1230 Ori	BD −5 1318	B8 IV–V	HAEBE	1	05 32 54	−05 23 00
52......	464	CQ Tau	HD 36910	A8veα	HAEBE	3	05 32 54.12	+24 43 03
53......	...	NT Ori	Haro 4–241	K8e	TTS	0	05 33 00	−06 49 48
54......	...	NU Ori	HD 37061	B1 V	HAEBE	5	05 33 03.75	−05 17 54.9
55......	...	V361 Ori	HD 37062	B4 V	HAEBE	1	05 33 03.96	−05 27 07.8
56......	471	NV Ori	Parenago 2086	F4, 8 III, V	NTTS	0	05 33 04.06	−05 35 01
57......	...	V566 Ori	BD −5 1328	A0 V	HAEBE	1	05 33 09	−05 14 18
58......	150	AN Ori	Parenago 2167	K0, 1 IV (Li)	HAEBE	1	05 33 14.56	−05 30 04
59......	154	T Ori	Haro 4–123	A3eα	HAEBE	2	05 33 23.05	−05 30 25
60......	482	BN Ori	HD 245465	F2, 3eα	HAEBE	5	05 33 47.65	+06 48 13
61......	483	Cohen–Schwartz star	...	G8:	CTTS	0	05 33 55.55	−06 47 25
62......	...	PR Ori	Haro 4–213	K4e	NTTS	0	05 33 58	−06 19 18
63......	164	V380 Ori	BD −6 1253	A1:e	HAEBE	5	05 33 59.50	−06 44 46
64......	167	Parenago 2441	...	G5: (Li)	CTTS	1	05 34 22.70	−04 27 26

TABLE 1—*Continued*

ID[a] (1)	HBC[b] (2)	Name[c] (3)	Alternate Name[c] (4)	Type[d] (5)	Category (6)	N[e] (7)	α (1950) (8)	δ (1950) (9)
65	169	BF Ori	Haro 4–229	A5e+sh	HAEBE	4	05 34 47.24	−06 36 45
66	170	RR Tau	AS 103	B8, 9eα	HAEBE	1	05 36 23.84	+26 20 49
67	...	HD 37490	Ω Ori	B3 III/IVe	HAEBE	10	05 36 32.61	+04 05 40.6
68	493	V350 Ori	...	B:e	HAEBE	0	05 37 49.32	−09 43 41
69	...	HD 37806	MWC 120	B9 Ve+sh	HAEBE	28	05 38 31.72	−02 44 28.8
70	...	V351 Ori	HD 38238	A7 III	HAEBE	2	05 41 44.89	+00 07 26.3
71	186	FU Ori	...	G:I, II	FU Ori	2	05 42 37.97	+09 03 02
72	192	HD 250550	MWC 789	B9eq	HAEBE	22	05 59 06.43	+16 30 59
73	193	LkHα 208	...	F0 Ve	HAEBE	1	06 04 53.17	+18 39 55
74	...	FS CMa	HD 45677	B3[e]p+sh	HAEBE	24	06 25 59.1	−13 01 12.0
75	202	VY Mon	...	B8:e	HAEBE	1	06 28 20.99	+10 28 14
76	528	LkHα 215	...	B7 IIne	HAEBE	1	06 29 56.1	+10 11 24
77	529	HD 259431	MWC 147	B5:e	HAEBE	5	06 30 19.4	+10 21 38
78	207	R Mon	BD +8 1427	...	HAEBE	3	06 36 26.05	+08 46 54
79	216	NX Mon	LHα 22	cont	CTTS	0	06 37 56.27	+09 36 48
80	219	V590 Mon	LHα 25	B8pe+sh	HAEBE	7	06 37 59.49	+09 50 53
81	...	HD 50138	MWC 158	B6 V[e]+sh	HAEBE	14	06 49 07.58	−06 54 21.6
82	...	OY Gem	HD 51585	B[e]	HAEBE	2	06 55 37.6	+16 23 32
83	...	GU CMa	HD 52721	B2 Vne	HAEBE	2	06 59 28.56	−11 13 41.4
84	243	Z CMa	HD 53179	B?eq pec	HAEBE	3	07 01 22.52	−11 28 36
85	...	HD 53367	MWC 166	B0 III/IVe	HAEBE	5	07 02 03.59	−10 22 43.7
86	...	EW CMa	HD 56014	B3 IIIep	HAEBE	1	07 12 12.83	−26 15 54.1
87	552	NX Pup	CoD −44 3318	F1:e	HAEBE	5	07 17 56.5	−44 29 35
88	...	HD 76534	He 3–225	B2/3ne	HAEBE	3	08 53 20.64	−43 16 29.7
89	...	HD 87643	He 3–365	B3/4[e]	HAEBE	9	10 02 49.72	−58 25 16.2
90	...	HD 94509	He 3–515	A0 Ve	HAEBE	1	10 51 25.02	−58 09 25.6
91	...	GG Car	HD 94878	B5/6[e]+K3:	HAEBE	11	10 53 58.01	−60 07 30.7
92	244	Sz 6	LHα 332–20	K2 (Li)	CTTS	0	10 57 50.8	−76 45 33
93	568	TW Hya	He 3–549	K7 V (Li)	CTTS	2	10 59 30.08	−34 26 07
94	...	HD 95881	He 3–554	A1/2 III/IVe	HAEBE	1	11 00 15.0	−71 14 43
95	569	CS Cha	Sz 9	K5:	CTTS	1	11 01 07.8	−77 17 25
96	...	HD 96675	CHXR 16	B6 IV/V	HAEBE	1	11 04 27.90	−75 51 35.5
97	245	LHα 332–17	HM 13	G2 V (Li)	CTTS	0	11 05 57.5	−77 21 50
98	575	VW Cha	Sz 24	K2	CTTS	1	11 06 38.1	−77 26 12
99	246	CU Cha	HD 97048	A0pe+sh	HAEBE	8	11 06 39.61	−77 23 01
100......	578	VZ Cha	Sz 31	K6	CTTS	0	11 07 51.9	−76 07 02
101......	...	HD 97300	CHXR 42	B9 V	HAEBE	4	11 08 18.07	−76 20 29.6
102......	588	Sz 41	HJM E1–9a	K0	CTTS	1	11 10 50.2	−76 20 45
103......	247	CV Cha	LHα 332–21	G8 V (Li)	CTTS	2	11 10 53.8	−76 28 01
104......	...	HD 98922	He 3–644	B9 Ve	HAEBE	3	11 20 13.05	−53 05 43.9
105......	...	HD 100546	He 3–672	B9 Vne	HAEBE	1	11 31 14.13	−69 55 06.9
106......	...	HD 104237	He 3–741	A4e	HAEBE	20	11 57 33.47	−77 54 50.5
107......	...	He 3–847	CPD −48 5215	...	HAEBE	0	12 58 24.3	−48 37 08
108......	...	He 3–1013	CPD −64 2939	Be	HAEBE	1	14 33 07.6	−64 35 02
109......	...	HD 132947	CPD −62 4379	A0e	HAEBE	1	15 00 48.37	−62 56 11.6
110......	248	Sz 68	CoD −33 10685	K2 V (Li)	CTTS	0	15 42 01.4	−34 08 08
111......	...	HD 141569	BD −03 3833	A0 Ve	HAEBE	0	15 47 20.21	−03 46 11.9
112......	...	HD 142361	ScoPMS 005	G2 IV	NTTS	2	15 52 01.2	−23 38 32.5
113......	251	RU Lup	Sz 83	K	CTTS	22	15 53 24.3	−37 40 35
114......	...	HD 142666	BD −21 4228	A7/8 Ve	HAEBE	1	15 53 43.26	−21 53 00.0
115......	608	HD 143006	He 3–1126	G5	CTTS	0	15 55 38.9	−22 48 46
116......	252	RY Lup	...	K0, 1 V (Li)	CTTS	2	15 56 05.0	−40 13 36
117......	...	ScoPMS 023	NTTS 155913–2233	K5 IV	NTTS	0	15 59 12.5	−22 33 09.5
118......	253	EX Lup	...	M0:V (Li)	CTTS	2	15 59 42.6	−40 10 09
119......	...	ScoPMS 027	NTTS 160153–1922	K2 IV	NTTS	0	16 01 53.5	−19 22 14.6
120......	612	HO Lup	Sz 88	M1	CTTS	1	16 03 39.4	−38 54 19
121......	...	HD 144432	He 3–1141	A7 Ve/F0e	HAEBE	2	16 03 53.56	−27 35 08.3
122......	616	HK Lup	Sz 98	K7, M0 (Li)	CTTS	1	16 05 00.9	−38 56 44
123......	617	Sz 102	THα 15–28	K?	CTTS	1	16 05 08.3	−38 55 16
124......	619	V856 Sco	HD 144668	A7e III, IV	HAEBE	23	16 05 12.78	−38 58 22
125......	254	V866 Sco A	AS 205	K5 V (Li)	CTTS	1	16 08 37.70	−18 30 42
126......	634	ScoPMS 052	Wa Oph/3	K0 IV (Li)	NTTS	1	16 09 46.37	−18 51 49
127......	...	ScoPMS 060	NTTS 161431–2256	G0 IV	NTTS	1	16 14 32.2	−22 56 14.8
128......	...	He 3–1191	WRA 15–1484	B0:[e]	HAEBE	1	16 23 31.0	−48 32 46
129......	264	AS 207	SR 9	K5, 7	CTTS	1	16 24 38.88	−24 15 23
130......	646	V346 Nor	HH57/IRS 8	F8eq III (Li)	FU Ori	0	16 28 56.8	−44 49 08

TABLE 1—*Continued*

ID[a] (1)	HBC[b] (2)	Name[c] (3)	Alternate Name[c] (4)	Type[d] (5)	Category (6)	N[e] (7)	α (1950) (8)	δ (1950) (9)
131......	...	HD 150193	MWC 863	A0/4 Ve	HAEBE	0	16 37 16.45	−23 47 56.4
132......	270	V1121 Oph	He 3–1260	K5 (Li)	CTTS	1	16 46 25.24	−14 16 56
133......	271	AK Sco	CoD −36 11056	F5 Ve (Li)	CTTS	3	16 51 23.12	−36 48 28
134......	655	V921 Sco	CoD −42 11721	Bep?	HAEBE	1	16 55 33.8	−42 37 37
135......	...	HD 326823	He 3–1330	B1.5[e]	HAEBE	1	17 03 20.3	−42 32 39.0
136......	273	KK Oph	THα 27–3	B, Ae	HAEBE	1	17 07 00.73	−27 11 36
137......	...	HD 327083	He 3–1359	B1.5e	HAEBE	0	17 11 45.9	−40 16 42
138......	...	He 3–1357	CPD −59 6926	B0/3e	HAEBE	3	17 11 56.29	−59 26 04.1
139......	...	He 3–1428	CD −49 11554	B0e	HAEBE	1	17 31 18	−49 24 18
140......	...	He 3–1475	...	Be	HAEBE	0	17 42 18.8	−17 55 36
141......	...	HD 316285	He 3–1482	B2/3[e]+sh	HAEBE	4	17 45 04.82	−27 59 55.2
142......	...	HD 163296	He 3–1524	A0/2 Vep+sh	HAEBE	64	17 53 20.65	−21 56 57.0
143......	662	V4046 Sgr	HD 319139	K5, 6 Vn (Li)	CTTS	8	18 10 53.69	−32 48 26
144......	664	FK Ser	BD −10 4662 A	K5 Vp (Li)	CTTS	2	18 17 37.02	−10 12 35
145......	282	VV Ser	IrCh 21	B, Ae	HAEBE	1	18 26 14.33	+00 06 39
146......	286	S CrA	...	K6:	CTTS	1	18 57 46.1	−37 01 37
147......	287	TY CrA	CoD −37 13024	B9	HAEBE	3	18 58 18.57	−36 56 18
148......	288	R CrA	...	A5:e+sh	HAEBE	2	18 58 31.6	−37 01 30
149......	678	Wa CrA/2	CoD −37 13029	G8 IV: (Li)	NTTS	1	18 58 39.0	−37 11 42
150......	...	HD 179218	MWC 614	B9/A0 IV/Ve	HAEBE	1	19 08 55.42	+15 42 15.1
151......	292	V1352 Aql	AS 353A	cont	CTTS	0	19 18 09.41	+10 56 14
152......	686	WW Vul	BD +20 4136	A0, 3Ve	HAEBE	2	19 23 49.01	+21 06 28
153......	...	V1295 Aql	HD 190073	A0 IVep+sh	HAEBE	5	20 00 34.43	+05 35 49.6
154......	689	V1685 Cyg	MWC 340	B2, 3e+sh	HAEBE	1	20 18 42.7	+41 12 18
155......	297	V751 Cyg	LkHα 170	A5:e	HAEBE	1	20 50 26.68	+44 08 05
156......	726	HD 200775	MWC 361	B3eq	HAEBE	7	21 00 59.70	+67 57 55
157......	730	BD +65 1637	...	B2, 3nne	HAEBE	2	21 41 41.1	+65 52 49
158......	309	LkHα 234	...	B5, 7e	HAEBE	1	21 41 57.60	+65 53 07
159......	310	BD +46 3471	AS 477	A4:e+sh	HAEBE	5	21 50 38.55	+46 59 35
160......	315	DI Cep	MHα 47–30	G8 V: (Li)	CTTS	8	22 54 08.18	+58 23 59
161......	317	MWC 1080	...	B0?eq	HAEBE	0	23 15 14.84	+60 34 19

NOTE.—Units of right ascension are hours, minutes, and seconds, and units of declination are degrees, arcminutes, and arcseconds.

[a] Internal identification number for cross-referencing.

[b] Catalog number from Herbig & Bell 1988.

[c] Names in Cols. (3) and (4) were selected with the following catalog precedence: variable star, HD, Bayer, Flamstead, HR, He, MWC, Haro, Sz, BD, SAO, CPD, WK, Parenago, MHα, LkHα, LHα, THα, LkCa, HH, AS, SR, DoAr, TAP, ScoPMS, Wa OPh, Wa CrA, CHXR, NTTS, L, JW, HM, HJM, St, CD, CoD, WRA, Hiltner, PC, W, ADS, IrCh, Bran, Eggen, SSS, PK, unique name.

[d] Spectral types preferentially from Herbig & Bell 1988 for TTS and Thé et al. 1994 for HAEBE stars.

[e] Number of *IUE* spectra. Multiple spectra per image counted explicitly. Not all spectra are usable.

Figure 1 demonstrates the relative quality of IUESIPS and NEWSIPS reductions of a single RU Lup spectrum, as well as the dramatic improvement in S/N ratios when all 22 available spectra are combined. NEWSIPS leaves fewer bad pixels (shown as gaps in Fig. 1) than IUESIPS, and in this case co-addition of several spectra removes all remaining bad pixels. Qualitatively, NEWSIPS processing roughly doubled the S/N ratio obtained from image SWP28851, especially at short wavelengths where the spectrum is faint. Combining all 22 NEWSIPS spectra improved S/N ratios by an extra factor of 3 or so. Quantitative assessment of S/N ratio gains is difficult in this case because the spectrum has no broad smooth sections, nor can the co-added spectrum be used as a low noise template because the line strengths are weaker in the combined spectrum, owing to actual stellar variation. Nichols & Linsky (1996) quantitatively assess the relative S/N ratio in co-added IUESIPS and NEWSIPS reductions of a continuum source. Figure 1 also shows the weighted mean of all 22 spectra processed with INES (Rodríguez-Pascual et al. 1999). The INES extraction produces a slightly enhanced C IV line, but the overall agreement between NEWSIPS and INES is generally quite good.

When archival spectra for a source vary widely in quality, the S/N ratio in the combined spectrum is not expected to scale simply with the number of exposures. Adding noisy spectra either does nothing (when using a noise-weighted mean) or reduces the S/N ratio (when using an unweighted mean). In the RU Lup example above, image SWP28851 was selected for its median S/N characteristics. The S/N ratio in the mean spectrum is predicted to be 5 times the S/N ratio in the individual spectrum shown, whereas the actual improvement was only a factor of 3. This is consistent with the noise characteristics described in Nichols & Linsky (1996). Formally, the "continuum" S/N ratio in the combined RU Lup spectrum ranges from 20–100 as wavelength increases, but the actual S/N ratio is probably only 10–50. As indicated in column (7) of Table 1, only 16 sources were observed at least 10 times, so co-addition will yield only modest S/N gains for most sources in our sample. On the other hand, even two spectra can be enough to fix all the bad pixels.

2.3. *Flux Variability*

By co-adding spectra, we average over potentially interesting temporal variations. Although a detailed analysis of

TABLE 2

SWP SEQUENCE NUMBERS FOR *IUE* OBSERVATIONS OF PRE–MAIN-SEQUENCE STARS

ID	SWP Sequence Numbers
1	53049[l]
2	02800, 09301[a]
3	30220, 37842, 37843[l]
4	24841[b,c]
5	55968[l]
6	34491[d]
7	48578[m]
8	07035,[b] 48829, 48903,[l] 48910[l]
9	14546,[m] 18954, 29345, 29346,[m] 29382, 29457, 29493, 39802, 43552, 43563, 43585, 43610, 43635, 43650, 43672, 43689
10	15340,[m] 18977, 32700
11	07034,[m,n] 21302, 21305, 21307, 21310, 25445, 26939, 27962, 29419, 30563, 35376, 35384, 35390, 35397
12	16321, 18244, 46987
13	03172,[n,o] 07006, 10543, 10600, 10613, 49799,[l] 49804[l]
14	35378,[p] 35386, 35392, 48853,[l] 48871,[l] 48893[l]
15	14590,[m] 15301, 16033
16	32183[o,q]
17	48629
18	49748

NOTES.—Table 2 appears in its entirety in the electronic edition of *The Astrophysical Journal*. A portion is shown here for guidance regarding its form and content. Information about spectra *included* in the weighted mean are indicated by footnotes "a" through "k." Information about spectra that were *excluded* from the weighted mean are indicated by footnotes "l" through "z."

[a] Fails one or more quality tests.
[b] Noisy spectrum.
[c] Classification uncertain.
[d] Questionable spectral feature at 1282 Å.
[e] Noisy spectrum; significance of spectral features is uncertain.
[f] Small-aperture spectrum is anomalously weak.
[g] Unusual continuum shape.
[h] Possible continuum detection.
[i] Questionable spectral feature near 1800 Å.
[j] Spectrum is unusable beyond 1700 Å.
[k] Spectrum is unusable beyond 1600 Å.
[l] Not available in final archive.
[m] No significant signal.
[n] Fails one or more quality tests.
[o] Very noisy spectrum.
[p] Small-aperture spectrum has no significant signal.
[q] C IV emission may be present.
[r] Small-aperture spectrum has questionable feature near 1250 Å.
[s] Small-aperture spectrum is anomalously strong.
[t] Spectrum is anomalously weak.
[u] Most or all of the spectrum is flagged as bad.
[v] Excessive contamination from nearby stars.
[w] Most or all of the small-aperture spectrum is flagged as bad.
[x] Small-aperture spectrum is anomalously weak.
[y] Noisy spectrum; significance of spectral features is uncertain.
[z] Questionable spectral feature at 1505 Å.

intrinsic variability is beyond the scope of this atlas, we have measured the amplitude and statistical significance of flux variations in the 72 stars with multiple spectra. This information in Table 4 may help to guide future investigations of temporal variability in individual stars.

Any procedure for characterizing variability in *IUE* spectra must properly account for the wide range of S/N ratios present in the archive. For each good spectrum in Table 2, we calculated the mean flux (F) in the wavelength interval 1250–1850 Å, ignoring pixels with data quality flags less than -15. We used the same set of pixels to calculate the mean flux ($F_{\rm sum}$) for the co-added spectrum. The quantity $\alpha = |F/F_{\rm sum} - 1|$ is a measure of the fractional change in flux for each individual spectrum relative to the co-added spectrum. We computed the fractional uncertainty (σ_α/α) in α by normal error propagation, except that we added an additional 5% uncertainty in quadrature to heuristically account for any residual errors in flux calibration. We then defined the fractional variability amplitude (A) as the weighted mean of α and obtained the formal uncertainty (σ_A) by normal error propagation. We characterized the significance of the variability by computing reduced χ^2, assuming as a model that there were no variations ($\alpha = 1$). Large χ_r^2 implies a poor model fit or, equivalently, the presence of significant variations. The quantity A/σ_A may also be used to judge significance.

Table 4 gives the results of the variability analysis ordered by decreasing χ_r^2. When the measured value of A is less than $2\sigma_A$, we present the result as an upper limit on A. Figure 2 shows A as a function of spectral type. For our biased sample, the largest UV flux variations are comparable for CTTS and HAEBE, despite very different contributions from quiescent photospheric emission. In cooler CTTS, emission from accretion and activity dominates quiescent photospheric flux, so UV variability is caused by stochastic variations in accretion rate, rotational modula-

TABLE 3

QUALITY INDICATORS FOR INDIVIDUAL SPECTRA

FITS Card	Good[a]	Description
CC-PERCN	>90%	Fraction of spectrum successfully cross correlated
CC-MEDN	>0.6	Median cross-correlation coefficient
SHIFTMEAN......	<0.5	Mean pixel shift from cross correlation
THDA*xxx*[b]	~9.3	Mean camera temperature (degrees C)
HISTORY[c]	<1	Measured |peak − centroid| of spectrum
HISTORY[c]	<2	|Observed − predicted| centroid of spectrum
HISTORY[c]	>3	Number of spline nodes defining spectrum shape
HISTORY[c]	<5	Number of pixels per wavelength bin
HISTORY[c]	<5	Calibration data extrapolated temporally
ABNBADSC	No	Bad scans occurred during read
ABNHISTR	No	Data recovered from history tape
ABNNOSTD.......	No	Data recorded in nonstandard manner
ABNOTHER.......	No	Corrupted image reconstruction
ABNREAD.........	No	Nonstandard read rate
ABNUVC	No	Nonstandard UVC voltage

[a] Expected values for "good" spectra.
[b] Mean during observation: (THDASTR + THDAEND)/2.
[c] HISTORY cards were parsed for specified information.

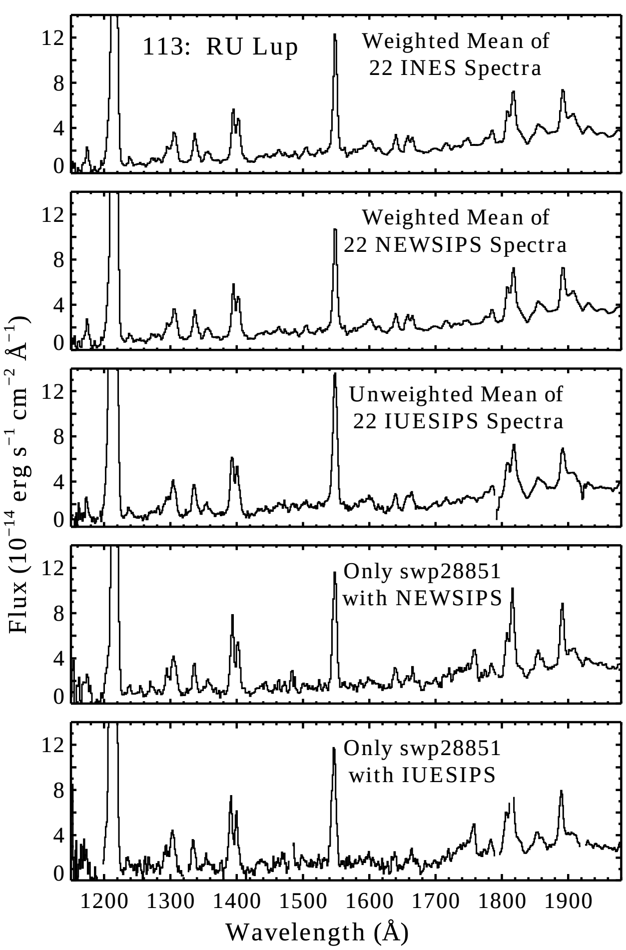

FIG. 1.—Comparison of RU Lup spectra processed in various ways. The bottom two panels illustrate how NEWSIPS can improve S/N ratios in individual *IUE* spectra relative to the older IUESIPS processing. The second and third panels show that this S/N advantage is maintained even when co-adding many spectra. The top two panels demonstrate that NEWSIPS and INES yield equivalent results.

tion of hot zones, and extinction variations. In HAEBE stars, localized heating is believed to have a relatively minor effect on UV emission, so the observed variability is more likely caused by changes in circumstellar absorption and extinction. Magnetic activity can affect NTTS, so variations are possible, but the evidence in Table 4 is not compelling since $A/\sigma_A \leq 4$ in all cases.

The variability amplitudes in Figure 2 lie below an upper envelope that appears to vary systematically with spectral type. This may be simply a manifestation of uncharacterizable sample selection effects, or there may be a

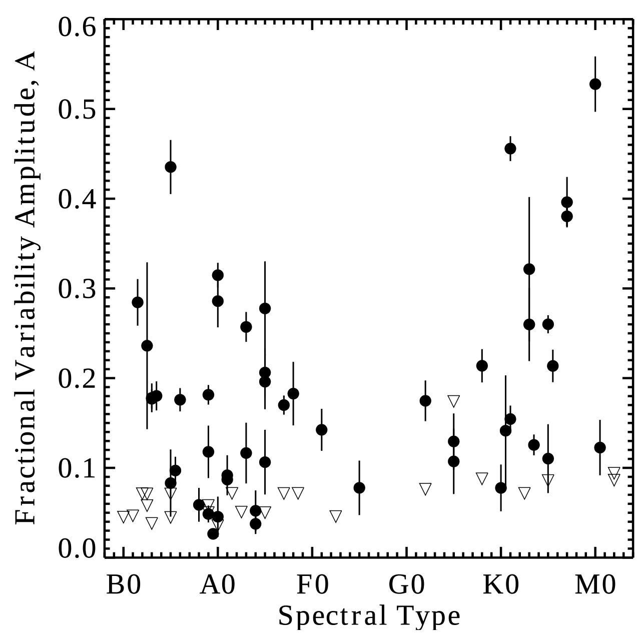

FIG. 2.—Mean variation in 1250–1850 Å flux, relative to the mean, for every PMS star observed more than once by *IUE*. Triangles indicates 2 σ upper limits. Values of A and σ_A are from Table 4. Spectral types are from Table 1.

TABLE 4

MEASURED FLUX VARIATIONS

ID[a]	Name	Category[b]	N[c]	χ_r^2	A[d]	σ_A
118	EX Lup	CTTS	2	472.5	52.8	3.1
93	TW Hya	CTTS	2	199.1	39.6	2.8
148	R CrA	HAEBE	2	196.0	27.8	5.3
35	RW Aur A	CTTS	8	185.1	45.6	1.4
84	Z CMa	HAEBE	3	129.1	43.5	3.0
9	BP Tau	CTTS	14	108.2	38.0	1.1
65	BF Ori	HAEBE	4	97.1	19.6	3.1
138	He 3–1357	HAEBE	3	83.3	28.4	2.6
34	UX Ori	HAEBE	11	74.4	25.7	1.7
27	DR Tau	CTTS	11	62.4	31.5	1.4
78	R Mon	HAEBE	3	59.2	28.6	2.9
29	GM Aur	CTTS	2	52.3	26.0	4.1
113	RU Lup	CTTS	22	51.9	26.0	1.0
52	CQ Tau	HAEBE	3	50.6	18.3	3.5
143	V4046 Sgr	CTTS	8	24.1	21.4	1.8
72	HD 250550	HAEBE	20	23.6	18.1	1.1
160	DI Cep	CTTS	8	23.4	21.4	1.9
89	HD 87643	HAEBE	9	21.3	18.0	1.6
67	HD 37490	HAEBE	10	20.7	17.8	1.6
37	HD 35929	HAEBE	4	20.1	20.6	2.7
81	HD 50138	HAEBE	14	19.9	17.6	1.3
11	RY Tau	CTTS	13	19.5	15.4	1.5
74	FS CMa	HAEBE	24	18.8	17.7	1.1
8	V410 Tau	NTTS	2	16.3	32.1	8.0
124	V856 Sco	HAEBE	23	14.8	17.0	1.1
38	GW Ori	CTTS	3	13.9	12.9	3.1
59	T Ori	HAEBE	2	12.6	11.7	3.4
32	SU Aur	CTTS	7	12.1	17.5	2.3
87	NX Pup	HAEBE	5	11.3	14.2	2.3
14	DF Tau	CTTS	3	10.6	12.3	3.1
40	HK Ori	HAEBE	2	9.7	10.6	3.6
2	V594 Cas	HAEBE	2	9.2	8.3	3.7
3	LkHα 264	CTTS	2	8.8	11.0	3.8
147	TY CrA	HAEBE	3	8.3	11.8	2.9
13	T Tau	CTTS	4	7.1	7.8	2.6
116	RY Lup	CTTS	2	7.0	14.1	6.2
142	HD 163296	HAEBE	66	6.0	8.7	0.6
12	HD 283572	NTTS	3	4.9	10.7	3.6
63	V380 Ori	HAEBE	5	4.7	9.2	2.2
141	HD 316285	HAEBE	4	4.5	23.6	9.3
91	GG Car	HAEBE	11	4.4	9.7	1.5
15	DG Tau	CTTS	2	3.6	<9.4	4.7
133	AK Sco	CTTS	3	3.4	7.8	3.0
159	AS 477	HAEBE	5	2.9	5.2	2.3
33	HD 31648	HAEBE	4	2.7	<5.1	2.5
144	FK Ser	CTTS	2	2.3	<8.6	4.3
80	V590 Mon	HAEBE	7	2.1	5.9	1.9
69	HD 37806	HAEBE	28	1.8	4.9	0.9
10	DE Tau	CTTS	2	1.7	<8.6	4.3
103	CV Cha	CTTS	2	1.6	<8.8	4.4
54	NU Ori	HAEBE	5	1.5	<4.6	2.3
153	V1295 Aql	HAEBE	5	1.1	4.6	2.2
104	HD 98922	HAEBE	3	0.8	<5.8	2.9
106	HD 104237	HAEBE	20	0.8	3.8	1.1
112	HD 142361	NTTS	2	0.6	<7.6	3.8
31	AB Aur	HAEBE	94	0.6	2.6	0.5
121	HD 144432	HAEBE	2	0.6	<7.2	3.6
156	HD 200775	HAEBE	7	0.5	<3.8	1.9
70	V351 Ori	HAEBE	2	0.2	<7.1	3.6
101	HD 97300	HAEBE	4	0.2	<5.0	2.5
85	HD 53367	HAEBE	5	0.2	<4.5	2.3
45	HD 245185	HAEBE	4	0.2	<5.0	2.5
60	BN Ori	HAEBE	5	0.2	<4.6	2.3
71	FU Ori	FUOri	2	0.1	<7.4	8.7
82	OY Gem	HAEBE	2	0.1	<7.1	3.5
99	CU Cha	HAEBE	8	0.1	<3.6	1.8
88	HD 76534	HAEBE	3	0.1	<5.8	2.9
77	HD 259431	HAEBE	5	0.1	<4.5	2.2
47	LL Ori	CTTS	2	0.0	<7.2	3.6
83	GU CMa	HAEBE	2	0.0	<7.1	3.6
152	WW Vul	HAEBE	2	0.0	<7.2	3.6
157	BD +65 1637	HAEBE	2	0.0	<7.1	3.6

[a] Identification number from Col. (1) of Table 1.
[b] PMS category from Col. (5) of Table 1.
[c] Number of good *IUE* spectra used in analysis.
[d] Relative amplitude of fluctuation (in percent).

physical origin worthy of further study. For the HAEBE stars, hotter stars might have a higher covering fraction of circumstellar clumps caused by enhanced mass loss or residual accretion in these relatively young stars. Several HAEBE stars were observed by *IUE* because they show strong optical variability. For CTTS, warmer stars have progressively more photospheric emission that might dilute accretion and activity variations.

3. RESULTS

3.1. *Spectral Atlas*

Figure 3 shows the combined *IUE* SWP spectra for every TTS in our sample. Stars are ordered by B1950 right ascension, as in Table 1, and labeled with an identification number and name from that table. The typeface for each label reflects whether the star was categorized as CTTS (roman type) or NTTS (italic type) in the column (6) of Table 1. Recall that some sources have no useful spectra (indicated by a zero in col. [7] of Table 1) and, hence, do not appear in Figure 3. All spectra are on the same wavelength scale, which is given at the bottom of each column. The flux scale factor of 10^{-14} ergs s^{-1} cm^{-2} Å^{-1} applies to all TTS spectra, though the flux range for each panel is given separately. TTS are faint enough that Lyα at 1216 Å in *IUE* spectra is dominated by geocoronal, rather than stellar, emission. To focus on stellar features, we ignored Lyα in choosing the plot ranges in Figure 3. A horizontal dashed line indicates the zero flux level, so that descenders can be used to visually estimate noise levels. Several of the spectra are dominated by noise, but all spectra show at least one real stellar feature.

Figure 4 is analogous to Figure 3 but shows the combined *IUE* SWP spectra for HAEBE stars ordered by spectral types determined in § 3.4. Names and identifying numbers again come from Table 1. Note, however, that the flux scale factor (10^{-13} ergs s^{-1} cm^{-2} Å^{-1}) is 10 times larger than in Figure 3. As expected, early B stars (No. 67, HD 37490, B3, for example) have continua that are still rising toward shorter wavelengths, whereas the cooler A stars (No. 37, HD 35929, A7, for example) have little or no detectable continuum flux shortward of 1500 Å. Between these limiting cases, continuum shapes in Figure 4 correlate approximately with literature spectral types in column (5) of Table 1, but there are exceptions (No. 80, V590 Mon, B8, looks like an early B star, for example), even allowing for the possible effects of extinction. Possible errors in spectral type are discussed further in § 3.4. Combined *IUE* SWP spectra may be obtained from http://sprg.ssl.berkeley.edu/~cmj/iue.html.

In addition to temperature-related variations in continuum shape, spectra in Figure 4 also show a wide variation in the strength of numerous broad absorption features near

1570, 1630, 1710, and 1850 Å. For example, note the progression of increasing line strength in HD 97300 (No. 101), AB Aur (No. 31), and HD 250550 (No. 72), despite very similar spectral types and continuum shapes. At a spectral resolution of 500 km s^{-1}, the distinction cannot be rotation. As discussed below, these absorption features are probably circumstellar and may be linked to accretion and/or mass loss.

3.2. *Line Identifications for T Tau and AB Aur*

Figure 5 shows the combined *IUE* spectrum of T Tau (No. 13), broken into two panels to allow adequate space for line identification. All of the identified atomic lines are strong chromospheric or transition-region lines observed in ordinary late-type stars, although TTS probably also have a significant contribution from accretion (Paper II). Sandlin et al. (1986) list atomic and molecular emission lines present in spectra of the solar limb, plage, umbral, and quiet regions. Comparing our *IUE* spectra with higher resolution archival spectra obtained with the Goddard High Resolution Spectrograph (GHRS), we were able to identify approximately 20 lines of H_2 present in UV spectra of TTS. Only the strongest of these lines or blends of lines are discernible in *IUE* spectra, but several TTS with H_2 have been observed in the UV only by *IUE*. Finally, hatched rectangles mark the wavelength extent of two pseudo-continuum regions, which cover the intervals 1755–1765 Å (" cnt 1760 ") and 1941–1975 Å (" cnt 1958 ").

Figure 6 shows the combined spectrum of the HAEBE star AB Aur (our No. 31), again broken into two panels. Unlike TTS, the lines in most HAEBE stars are in absorption. Since the absorption lines have ionization states ranging from C I through at least N V, the spectrum cannot form exclusively in the stellar photosphere. Absorption lines may also form in interstellar or circumstellar (outflowing or accreting) material, as has been demonstrated with higher resolution optical, *IUE*, and GHRS spectra (Praderie et al. 1986; Blanco, Fonti, & Strafella 1988; Böhm et al. 1996; Bouret, Catala, & Simon 1997; Bouret & Catala 1998; Grady et al. 1999a). The line identifications in Figure 6 are drawn from these references. Blondel, Talavera, & Djie (1993) have argued that Lyα emission seen in high-dispersion *IUE* spectra of five HAEBE stars and two CTTS is an indication of accretion. As discussed by Landsman & Simon (1993), geocoronal contamination can be removed from low-dispersion *IUE* spectra, but this involves fitting image data with a two-dimensional Lyα profile, which is beyond the scope of this project. Also, conversion to intrinsic stellar fluxes would depend on the poorly known interstellar extinction toward each star.

To search for HAEBE specific absorption features in AB Aur, we compared the spectrum of AB Aur with a spectral type sequence of dwarf B and A type stars observed with *IUE*. Construction of *IUE* template spectra for main-sequence standards followed the same basic procedure used for the PMS stars and is detailed in § 3.4. Although the

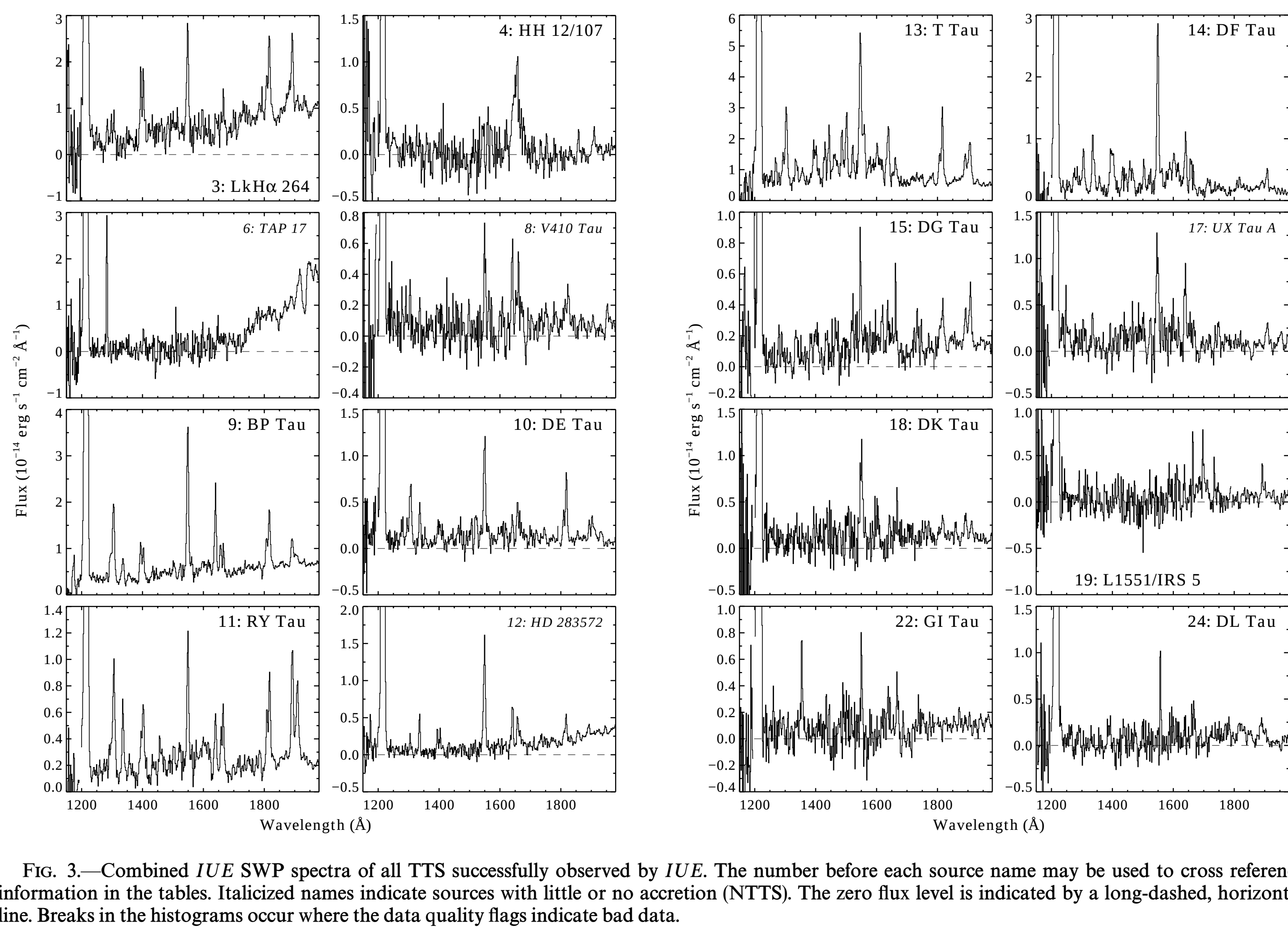

FIG. 3.—Combined *IUE* SWP spectra of all TTS successfully observed by *IUE*. The number before each source name may be used to cross reference information in the tables. Italicized names indicate sources with little or no accretion (NTTS). The zero flux level is indicated by a long-dashed, horizontal line. Breaks in the histograms occur where the data quality flags indicate bad data.

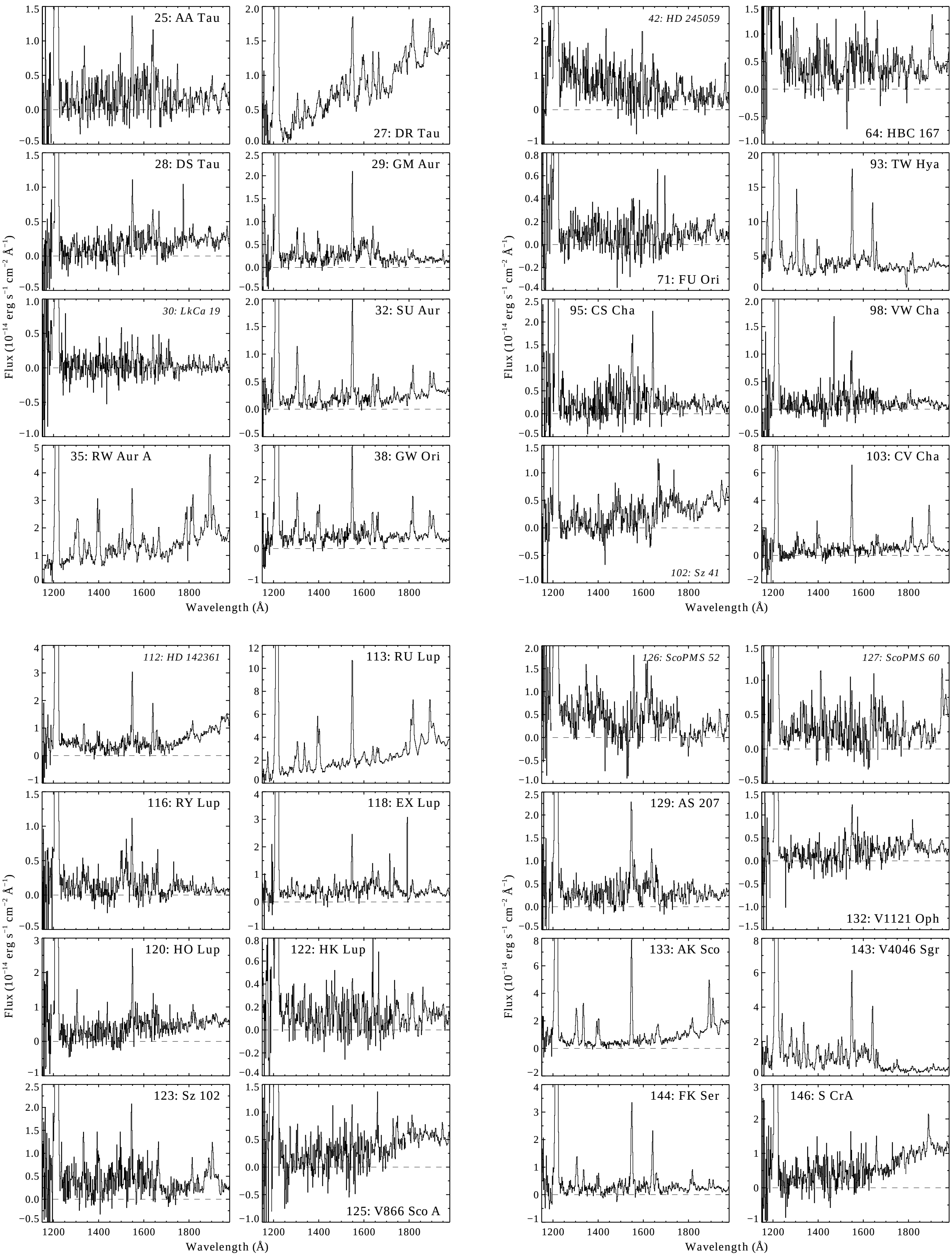

FIG. 3.—*Continued*

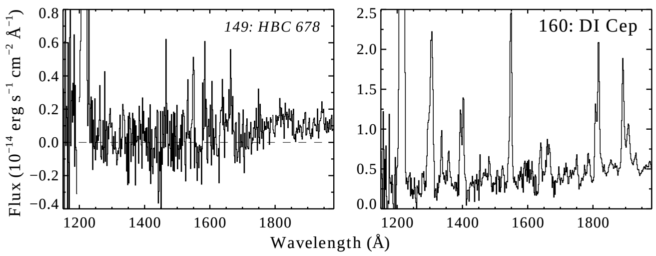

FIG. 3.—*Continued*

spectral class of AB Aur is "B9, A0e+sh", we obtained a better match using an average of HD 48915 (Sirius, A1 V) and HD 97633 (A2 V) with a reddening of $A(V) = 0.38$. The resulting normal template for AB Aur is shown along with AB Aur in Figure 6. Broad HAEBE specific absorption features are present exclusively in AB Aur at 1560–1580, 1600–1650, 1680–1730, and 1850–1870 Å. As discussed in § 3.4, many other HAEBE stars in Figure 4 show these same broad features, which separate into individual lines of Fe II, Al II, and other species at higher spectral resolution.

3.3. *Emission-Line Fluxes*

For the TTS that appear in Figure 3, we have measured several continuum and composite line fluxes, which are given in Tables 5 and 6. Identification numbers in the first column refer back to Table 1 and to the labels in Figure 3. The second and third columns give weighted mean continuum fluxes in the wavelength intervals 1755–1765 Å ("cnt 1760") and 1941–1975 Å ("cnt 1958"). Subsequent columns give integrated fluxes for groups of lines, as described below.

After each measured flux in Tables 5 and 6, parentheses enclose the 1 σ uncertainty in the last two tabulated digits. For example, "7.4 (0.4)" at the top of the second column corresponds to a continuum flux of $(7.4 \pm 0.4) \times 10^{-15}$ ergs s^{-1} cm^{-2} Å^{-1}, whereas "7.78 (46)" at the bottom of the fourth column corresponds to an integrated line flux of $(7.78 \pm 0.46) \times 10^{-14}$ ergs s^{-1} cm^{-2}. For spectral features with measured fluxes less than twice the estimated uncertainty, we tabulate 2 σ upper limits preceded by a "$<$" sign. No value is tabulated when the spectrum had no apparent flux in the relevant wavelength interval.

Given the diversity of the TTS spectra in Figure 3, we needed a variety of techniques to measure line fluxes. First, we removed a linear or quadratic pseudo-continuum, interactively fitted to regions that appeared relatively free of emission lines. Once the continuum was removed, we simply added all flux between two interactively specified integration limits. If the emission feature looked like a superposition of no more than a few Gaussian curves, we also interactively fit one or more Gaussian functions to

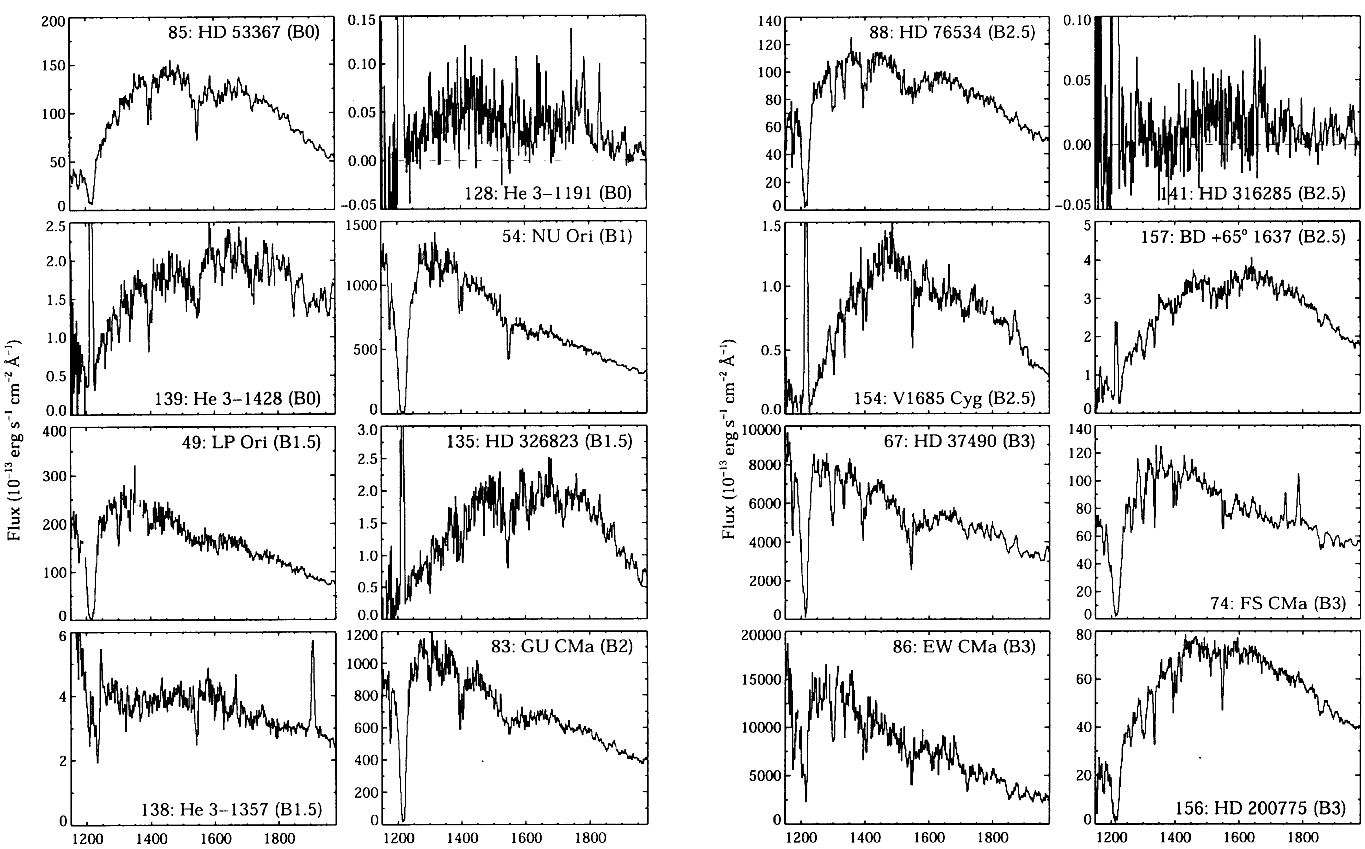

FIG. 4.—Combined *IUE* SWP spectra of all Herbig Ae/Be stars successfully observed by *IUE*, ordered by spectral type. The number before each source name may be used to cross reference information in the tables. The zero flux level is indicated by a long-dashed, horizontal line. Breaks in the histograms occur where the data quality flags indicate bad data.

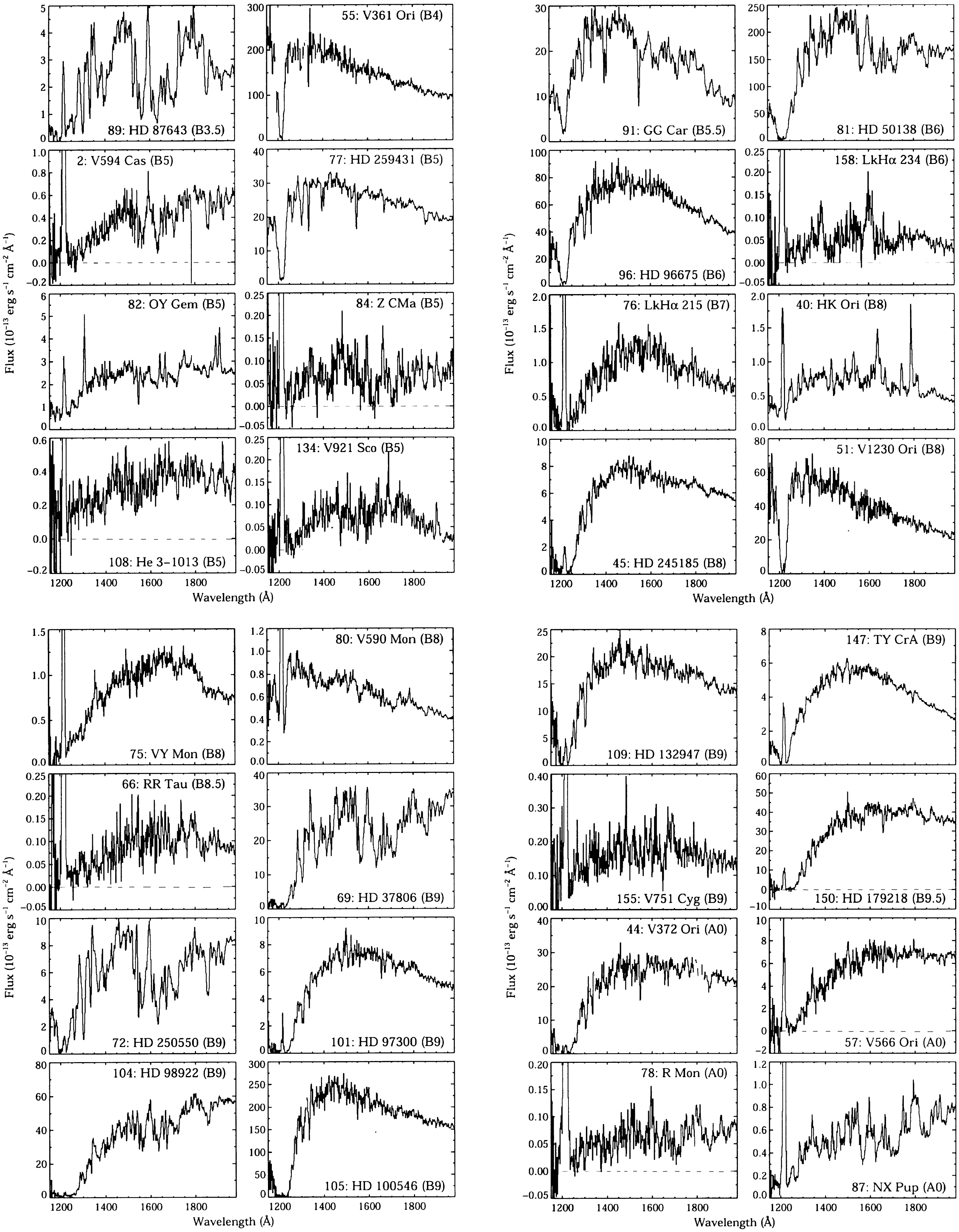

FIG. 4.—*Continued*

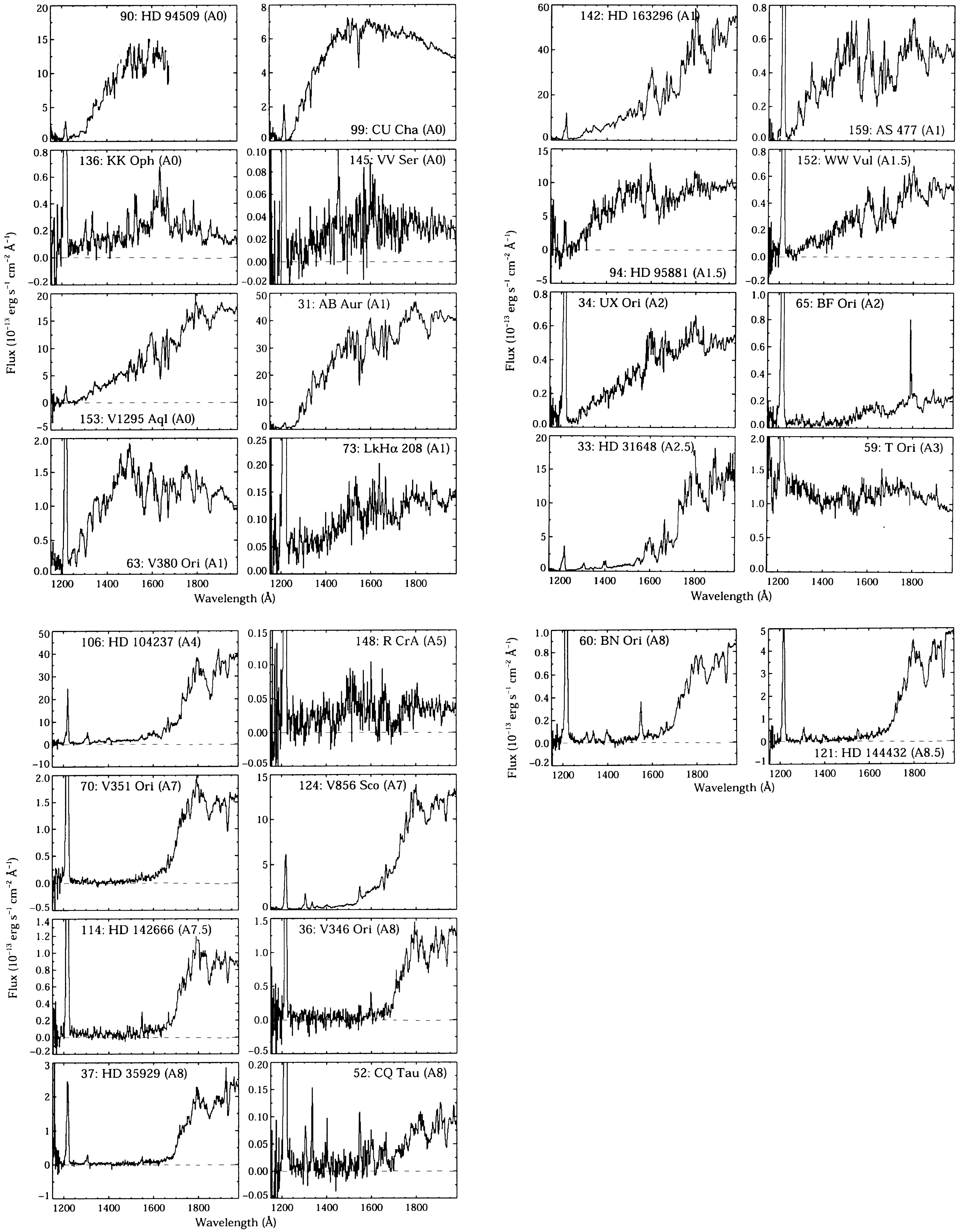

FIG. 4.—*Continued*

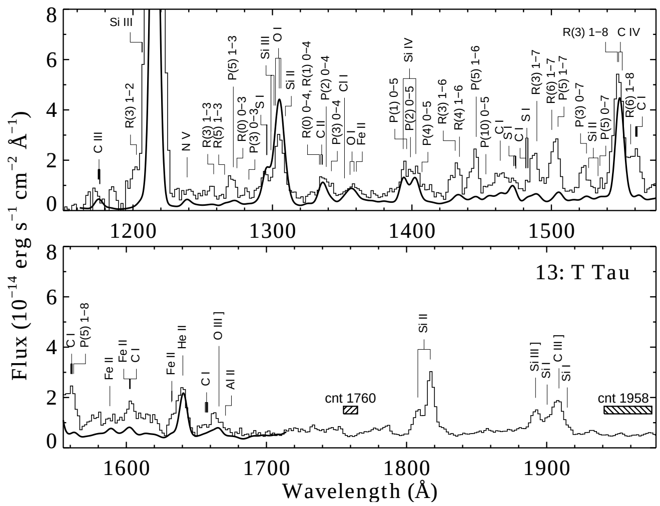

FIG. 5.—Combined *IUE* SWP spectrum of the classical TTS T Tau (*histogram*) and the montage of two GHRS G140L spectra (*dark curve*) degraded to the resolution of *IUE*. Emission-line identifications are given for atomic ions and for fluoresced H_2 transitions. The combined *IUE* spectrum generally has more flux, particularly in the H_2 lines. We believe this is caused by the larger aperture of *IUE*, implying that the H_2 emission is extended on scales significantly larger than 0″.2.

the specified segment of spectrum, using the area under the fit as a second line flux estimate. If the overlap between neighboring Gaussian curves was not too severe, the flux was apportioned into appropriate subintervals. Finally, for most spectral segments, we automatically fit Gaussian functions with predetermined wavelength separations, allowing only the amplitudes and a global shift to vary. The area under these automatic fits yielded our third and final flux measure. In general, we prefer the automatically determined line fluxes, followed by the interactively fitted Gaussian fluxes, and resorted to simple summation only for a few poorly behaved spectral segments. Visual inspection of all fits and flux determinations was made to guard against any obvious errors in the procedure.

Beginning with the fourth column of Table 5, the following methods were used to determine the tabulated fluxes.

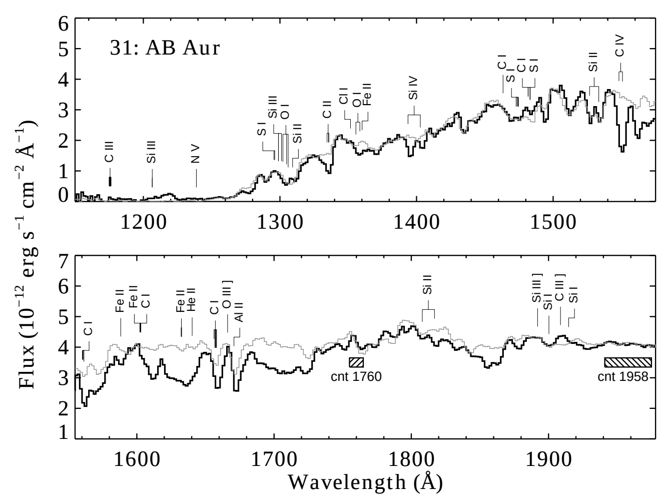

FIG. 6.—Combined *IUE* SWP spectrum of the Herbig Ae/Be star AB Aur (*dark histogram*) and a main-sequence comparison spectrum (*light histogram*) constructed as described in the text. AB Aur has broad circumstellar features longward of 1560 Å that are not present in the template spectrum.

Four Gaussian lines were automatically fitted to S I 1296.2, O I 1302.2, O I 1305.4, and Si II 1309.3 Å, with the sum of the two O I components comprising the "O I 1304" column of Table 5. Three Gaussian lines were automatically fitted to Si IV 1393.8, H_2 P (2) 0–5 1399.0, and Si IV 1402.8 Å, but only the fluxes for the two Si IV lines are tabulated. The four H_2 columns in Tables 5 and 6 contain interactively determined fluxes covering the wavelength intervals 1418–1438, 1438–1457, 1496–1513, and 1513–1534 Å with the corresponding column heading indicating the wavelength of the strongest H_2 line in the interval (see below). For some stars, the "H_2 1530" flux may also contain a significant contribution from Si II 1526.7 and 1533.4 Å. The "C IV 1549" column in Table 6 contains interactively determined fluxes for the wavelength interval 1534–1555 Å, which in some cases includes emission from H_2 R (3) 1–8 1547.3 Å. Interactive fitting covering the wavelength interval 1627–1648 Å was used to determine the "He II 1640" flux, which includes significant contributions from a pair of moderately strong Fe II lines. The Si II 1808.0 and Si II 1816.9 Å lines were automatically fitted together but are tabulated separately. Finally, four Gaussian lines were fitted to Si III] 1982.0, S I 1900.3, C III] 1908.7, and S I 1914.7 Å, but only the fluxes from the Si III] and C III] components are included in Table 6.

Given the low spectral resolution of *IUE*, each line flux in Tables 5 and 6 also includes contributions from weak blends. For a few stars, *HST* spectra allow individual line fluxes to be resolved, thus providing a rough estimate of the general contamination likely to be present in *IUE* spectra. For example, Fe II in DF Tau contributes about 13% of the total flux in our "He II 1640" integration range, though this fraction rises to 20% of the distinct line flux once we subtract the pseudo-continuum.

We also have used archival *HST* spectra to identify the strongest H_2 lines present in UV spectra of TTS. In particular, our "C IV 1549" flux includes a contribution from the H_2 R (3) 1–8 transition at 1547.3 Å. The magnitude of this contamination can be estimated by examining other H2 lines from the same Lyα pumped state ($J = 4$, $v = 1$), namely, P (5) 1–6 1446.1 in the "H_2 1433" interval and P (5) 1–7 1504.8 in the "H_2 1503" interval. Abgrall et al. (1993) gives relative oscillator strengths of 1.3, 1.8, and 1.0 for the H_2 transitions at 1446, 1505, and 1547 Å. Accurately measured fluorescent line fluxes will scale accordingly.

In a large-aperture GHRS spectrum of T Tau, roughly half of the flux in each "H_2" interval is from the main H_2 transition, but that fraction likely depends on stellar properties and spectrograph aperture. Nonetheless, our measured "H_2 1503" flux is certainly an upper limit on the actual P (5) 1–7 flux. Scaling this measured flux by the ratio of oscillator strengths (0.55) gives an upper limit on contamination of our measured "C IV 1549" flux by H_2 R (3) 1–8. For the 12 stars with both flux measures, we find contamination fractions ranging from $5 \pm 2\%$ (V4046 Sgr) to $47 \pm 8\%$ (DR Tau) with a mean of 10%, a median of 12%, and a standard deviation of 13%. If the GHRS spectrum of T Tau is typical, the actual contamination (and its variation from star to star) would be a factor of 2 lower.

As a final check on the H_2 scaling analysis, we compared our "H_2 1433" and "H_2 1503" fluxes for the four stars with both measurements. Assuming the main H_2 line dominates in each wavelength interval, we expect a flux ratio of 0.70. The observed ratio is actually 0.57 ± 0.03 with one anomalously low ratio (0.27 ± 0.07) for BP Tau, which has by far

TABLE 5

MEASURED FLUXES FOR T TAURI STARS

ID	cnt 1760 10^{-15}	cnt 1958 10^{-15}	S I 1296 10^{-14}	O I 1304 10^{-14}	Si II 1309 10^{-14}	Si IV 1394 10^{-14}	Si IV 1403 10^{-14}	H_2 1433 10^{-14}	H_2 1450 10^{-14}
3	7.4 (0.4)	9.61 (18)	5.1 (1.3)	4.8 (2.1)	<2.86	9.8 (1.5)	9.0 (1.5)	...	...
4	<0.82	0.57 (16)	<0.94	<1.38	<0.95	<0.53	<0.55	...	...
6	4.9 (0.4)	17.72 (13)	<0.66	<0.94	0.75 (33)	<0.66	2.51 (33)	...	...
8	<0.50	0.92 (10)	0.82 (22)	1.98 (32)	<0.44	0.83 (19)	0.56 (19)	...	...
9	6.0 (0.1)	6.67 (04)	6.48 (26)	11.78 (61)	6.95 (46)	4.86 (25)	3.91 (26)	0.92 (21)	.61 (1)7)
10	0.6 (0.1)	0.59 (05)	1.88 (32)	3.19 (93)	3.09 (67)	1.04 (25)	0.57 (26)	...	...
11	1.9 (0.1)	2.07 (03)	2.59 (17)	5.82 (45)	3.14 (36)	1.64 (07)	2.90 (07)	...	...
12	1.4 (0.2)	3.32 (07)	0.28 (11)	1.08 (17)	0.57 (12)	1.71 (10)	1.59 (10)	...	...
13	4.8 (0.2)	5.19 (09)	10.77 (57)	16.9 (1.7)	10.9 (1.1)	7.34 (59)	5.9 (0.6)	9.2 (0.6)	12.2 (0.7)
14	2.0 (0.2)	1.43 (06)	2.31 (31)	5.29 (75)	2.23 (67)	4.44 (12)	3.33 (12)	...	...
15	0.7 (0.2)	1.54 (07)	<0.77	<1.43	<1.02	1.36 (23)	1.08 (23)	...	...
17	<0.60	1.13 (12)	<1.16	<1.64	<1.16	<2.11	<2.87	...	...
18	1.7 (0.3)	0.90 (12)	<1.54	<2.18	<1.54	1.50 (39)	1.23 (39)	...	...
19	<0.62	0.30 (12)	<0.46	<0.65	<0.46	<0.46	<0.46	...	...
22	1.0 (0.3)	1.33 (11)	1.20 (34)	<0.96	<0.68	<1.19	<1.71	...	...
24	0.9 (0.3)	0.38 (13)	<0.45	<0.64	<0.45	1.56 (44)	<0.88	...	...
25	<1.11	2.40 (22)	<1.36	2.44 (96)	<1.36	<1.39	<1.39	...	...
27	11.4 (0.1)	14.35 (04)	2.96 (25)	3.55 (58)	3.63 (39)	2.50 (14)	2.67 (14)	...	...
28	2.1 (0.3)	2.94 (11)	<0.53	1.07 (37)	<0.52	1.40 (30)	<0.60	...	...
29	1.5 (0.2)	1.68 (07)	1.27 (32)	4.69 (49)	1.68 (34)	2.58 (58)	<1.04	...	...
30	<0.57	0.44 (11)	<0.94	<1.33	<0.94	<0.59	1.84 (29)	...	...
32	1.6 (0.1)	3.24 (05)	2.39 (27)	7.23 (76)	2.98 (73)	1.31 (31)	1.55 (48)	...	...
35	13.5 (0.2)	16.40 (10)	12.45 (53)	14.26 (76)	15.61 (53)	12.89 (54)	10.7 (0.5)	2.9 (0.8)	4.2 (0.6)
38	2.6 (0.2)	2.47 (08)	5.42 (47)	9.43 (74)	5.01 (51)	5.39 (65)	6.2 (0.7)	...	...
42	8.1 (0.7)	2.43 (28)	8.1 (3.0)	<8.62	7.9 (3.0)	<2.46	3.6 (1.2)	...	...
64	2.5 (0.5)	3.97 (22)	...	...	...	...	...	...	...
93	30.5 (0.6)	35.59 (23)	30.1 (1.7)	82.7 (5.3)	40.6 (4.3)	24.3 (2.0)	23.4 (2.2)	...	...
95	0.8 (0.4)	1.48 (13)	<1.71	<2.42	2.13 (85)	<1.71	<1.71	...	...
98	<0.49	0.61 (10)	0.92 (36)	<1.00	<0.71	<0.71	1.34 (36)	...	...
102	4.6 (0.5)	6.13 (20)	2.48 (57)	<1.62	2.48 (57)	<1.62	3.1 (0.9)	...	...
103	3.9 (0.5)	3.50 (20)	3.1 (1.2)	10.1 (2.5)	<4.89	9.85 (84)	9.4 (0.8)	...	...
112	5.2 (0.3)	13.56 (09)	3.63 (71)	3.6 (1.3)	3.50 (81)	3.27 (44)	2.51 (44)	...	...
113	23.1 (0.2)	34.75 (07)	16.86 (74)	22.3 (1.2)	16.29 (84)	27.22 (68)	19.8 (0.7)	...	...
116	1.1 (0.2)	0.64 (09)	<1.04	1.77 (74)	<1.05	<1.02	<1.48	...	...
118	4.2 (0.3)	2.84 (12)	<1.75	5.01 (66)	3.20 (46)	2.33 (19)	3.85 (19)	...	...
120	4.0 (0.5)	5.67 (20)	2.27 (71)	7.5 (1.0)	<1.43	<1.52	2.6 (0.8)	...	...
122	<0.67	1.14 (13)	...	...	...	...	...	...	...
123	2.2 (0.4)	2.59 (16)	2.36 (94)	<4.47	3.3 (1.4)	3.79 (90)	4.8 (0.9)	...	...
125	4.2 (0.4)	5.32 (18)	<0.89	3.40 (63)	1.44 (45)	3.09 (45)	2.14 (45)	...	...
126	3.4 (0.5)	1.94 (17)	...	...	...	...	...	...	...
127	1.4 (0.5)	6.15 (21)	...	...	...	...	...	...	...
129	2.8 (0.4)	2.93 (18)	<2.63	<3.73	<2.64	<1.27	<1.27	...	...
132	2.4 (0.5)	2.74 (16)	1.48 (73)	<2.14	2.09 (74)	1.81 (40)	1.96 (40)	...	...
133	7.1 (0.3)	19.32 (15)	6.34 (84)	19.8 (2.0)	9.0 (1.6)	10.16 (86)	13.1 (1.0)	...	...
143	4.3 (0.2)	3.64 (09)	5.24 (73)	14.2 (1.4)	4.2 (1.5)	9.14 (72)	7.2 (0.8)	8.2 (0.9)	11.5 (0.8)
144	2.3 (0.3)	1.60 (10)	1.82 (48)	9.7 (1.2)	2.63 (95)	4.20 (29)	3.50 (28)	...	...
146	7.8 (0.5)	11.24 (20)	<3.33	<4.73	<3.34	5.8 (2.1)	<4.37	...	...
149	0.6 (0.2)	1.25 (07)	1.09 (28)	<0.79	<0.56	<0.56	<0.56	...	...
160	3.2 (0.2)	5.04 (07)	7.78 (46)	13.9 (1.0)	10.28 (72)	5.97 (30)	6.16 (30)	...	...

NOTE.—Values in each column must be multiplied by the factor at the top of each column. Continuum spectral fluxes are in units of ergs^{-1} s^{-1} cm^{-2} Å^{-1}. Integrated line fluxes are in units of ergs^{-1} s^{-1} cm^{-2}. Uncertainties in the last two digits are enclosed in parentheses after each value. Tabulated upper limits are twice the measured uncertainty. The absence of a measurement indicates that the line was not apparent in the spectrum. Line fluxes in several of columns include more than one significant contributor.

the weakest "1433" flux. Excluding BP Tau yields a ratio of 0.65 ± 0.04, which is consistent with the ratio of oscillator strengths. Either way, the scaling analysis is accurate enough to estimate contamination.

In Paper II, we convert our measured "C IV 1549" fluxes to stellar surface fluxes and compare with other interesting stellar properties. Contamination from H_2 will introduce typical errors of 5% and worst-case errors as large as 25%. These errors are small, however, when compared to the broad range of inferred surface fluxes, which spans 2 orders of magnitude.

Finally, HAEBE stars later than spectral class A2 have relatively weak photospheric continua at wavelengths below 1600 Å. Atomic emission lines that are strong in spectra of TTS also appear in relatively cool HAEBE stars. We measured emission-line fluxes for nine HAEBE stars in our sample, following exactly the procedure described above for TTS. Resulting line fluxes are given in Table 7,

TABLE 6

More Measured Fluxes for T Tauri Stars

ID	H_2 1503 10^{-14}	H_2 1530 10^{-14}	C IV 1549 10^{-13}	He II 1640 10^{-14}	Si II] 1808 10^{-14}	Si II] 1817 10^{-14}	Si III] 1892 10^{-14}	C III] 1909 10^{-14}
3	...	...	1.96 (31)	...	6.1 (1.2)	12.2 (1.2)	12.1 (1.2)	<2.32
4	...	...	...	...	<0.75	<0.74	<0.69	1.3 (0.5)
6	...	...	...	...	<0.66	<0.66	<0.66	<0.66
8	...	...	0.38 (05)	3.29 (05)	1.24 (19)	1.92 (19)	<0.53	0.59 (27)
9	2.55 (33)	.42 (25)	2.52 (04)	12.68 (03)	4.51 (15)	8.61 (15)	4.11 (17)	1.36 (17)
10	...	...	0.91 (05)	1.88 (04)	2.10 (16)	4.90 (16)	1.43 (16)	1.01 (16)
11	...	...	0.87 (03)	3.82 (02)	3.16 (07)	5.16 (07)	6.66 (11)	4.44 (10)
12	...	...	1.17 (05)	4.27 (04)	0.51 (16)	2.11 (18)	1.02 (17)	<0.33
13	18.2 (0.7)	8.9 (0.7)	4.45 (09)	17.4 (0.7)	6.44 (29)	15.84 (31)	6.81 (28)	9.73 (30)
14	3.69 (34)	1.84 (27)	2.23 (06)	8.19 (04)	1.39 (12)	1.97 (12)	1.67 (17)	2.82 (18)
15	...	...	0.50 (06)	2.45 (04)	1.43 (23)	2.40 (23)	1.77 (28)	2.66 (30)
17	...	...	1.04 (10)	6.6 (0.7)	<0.46	0.65 (23)	<0.46	1.58 (23)
18	...	...	0.91 (11)	1.6 (0.6)	0.98 (38)	2.00 (38)	1.98 (38)	0.86 (38)
19	...	...	...	...	<0.45	<0.45	1.83 (29)	<0.56
22	...	...	0.44 (08)	2.5 (0.7)	<0.67	<0.67	<0.67	<0.67
24	...	...	...	<0.62	<0.69	1.57 (35)	1.65 (34)	<0.68
25	...	...	0.84 (15)	6.3 (0.6)	<1.58	<1.55	<1.54	<1.55
27	7.84 (45)	6.87 (45)	1.73 (06)	4.96 (02)	3.66 (14)	5.79 (14)	4.12 (17)	2.96 (17)
28	...	...	0.62 (08)	4.4 (0.8)	0.79 (35)	1.48 (36)	1.32 (33)	<0.66
29	1.08 (38)	1.67 (39)	1.15 (06)	5.0 (0.5)	1.34 (20)	1.33 (20)	0.57 (20)	<0.40
30	...	...	0.22 (07)	2.1 (0.6)	<0.65	0.98 (33)	0.83 (23)	1.42 (23)
32	3.12 (30)	2.36 (27)	1.49 (04)	4.61 (03)	1.92 (09)	4.00 (09)	2.65 (08)	2.51 (08)
35	8.9 (0.9)	5.8 (1.0)	2.09 (10)	2.8 (0.6)	9.7 (0.5)	13.4 (0.5)	...	...
38	1.6 (0.6)	...	1.90 (10)	6.6 (1.0)	3.55 (43)	8.36 (46)	5.74 (43)	4.72 (43)
42	...	...	<0.41	6.0 (1.8)	<2.76	3.7 (1.4)	2.7 (1.3)	<2.63
64	...	...	...	...	...	...	...	...
93	11.4 (1.5)	10.9 (1.5)	12.29 (40)	69.9 (1.2)	6.3 (1.1)	14.5 (1.1)	3.6 (1.1)	7.8 (1.1)
95	...	...	1.24 (23)	10.1 (1.2)	<1.75	<1.75	<1.71	<1.71
98	...	...	0.78 (12)	...	1.41 (35)	<0.70	0.73 (35)	<0.70
102......	...	...	<0.28	...	<1.15	<1.15	<1.38	<1.41
103......	...	...	4.10 (24)	5.0 (1.8)	6.7 (1.0)	14.9 (1.0)	23.0 (1.1)	6.2 (1.0)
112......	...	...	1.95 (12)	8.6 (0.7)	1.84 (44)	3.45 (44)	<0.88	<0.88
113......	7.9 (1.3)	5.5 (1.1)	7.63 (11)	11.2 (0.9)	21.0 (0.7)	31.5 (0.7)	29.6 (0.7)	12.5 (0.7)
116......	5.5 (0.7)	5.0 (0.6)	0.64 (07)	1.75 (04)	0.96 (21)	1.20 (21)	<0.41	1.33 (21)
118......	...	...	1.44 (08)	9.1 (0.7)	1.59 (34)	3.97 (35)	4.38 (19)	1.23 (19)
120......	...	...	1.21 (15)	3.8 (1.2)	<1.65	3.0 (0.9)	<1.42	<1.42
122......	...	...	...	...	...	...	...	...
123......	...	...	1.24 (15)	3.5 (1.0)	1.3 (0.6)	4.4 (0.6)	4.8 (0.6)	6.8 (0.6)
125......	...	...	0.50 (13)	...	<1.16	3.2 (0.6)	<0.88	<0.88
126......	...	...	...	...	...	...	...	...
127......	...	...	...	...	...	...	...	...
129......	...	...	1.95 (17)	8.9 (1.7)	<1.54	2.6 (0.7)	<1.26	<1.26
132......	...	...	0.77 (13)	...	2.66 (40)	4.22 (40)	<0.80	<0.80
133......	...	...	5.48 (14)	3.7 (1.0)	4.6 (0.5)	8.4 (0.5)	26.2 (0.6)	15.1 (0.6)
143......	16.4 (0.9)	12.2 (1.0)	4.72 (10)	30.5 (0.9)	<1.00	1.72 (50)	<0.92	2.25 (46)
144......	...	...	2.75 (11)	16.7 (0.8)	2.66 (24)	4.99 (25)	2.42 (28)	2.21 (28)
146......	...	...	<0.73	...	<3.30	<3.30	7.9 (1.7)	<3.39
149......	...	...	<0.19	...	0.59 (28)	0.92 (28)	<0.55	<0.55
160......	<0.78	1.6 (0.5)	1.72 (09)	3.4 (0.5)	5.95 (30)	11.40 (30)	9.73 (34)	4.17 (33)

Note.—Values in each column must be multiplied by the factor at the top of each column. Continuum spectral fluxes are in units of $ergs^{-1}\ s^{-1}\ cm^{-2}\ Å^{-1}$. Integrated line fluxes are in units of $ergs^{-1}\ s^{-1}\ cm^{-2}$. Uncertainties in the last two digits are enclosed in parentheses after each value. Tabulated upper limits are twice the measured uncertainty. The absence of a measurement indicates that the line was not apparent in the spectrum. Line fluxes in several of columns include more than one significant contributor.

which is analogous to Tables 5 and 6 for TTS, except that fewer lines appear and the scale factors for some columns are larger.

3.4. *HAEBE Absorption and Extinction*

Figure 6 shows broad absorption features present in the co-added spectrum of AB Aur but not in a main-sequence template of the same spectral type. As illustrated in Figure 7, these absorption features vary in strength, even within a single spectral type. This suggests that the absorption is circumstellar, rather than photospheric, in origin. As a prelude to further investigation at higher spectral resolution, we have used our co-added spectra to characterize the strength of the absorption features for all HAEBE stars observed with *IUE*. With these data, it is difficult to define a physically meaningful line absorption index, but a semiquantitative indicator of line depth is useful nonetheless.

TABLE 7

MEASURED LINE FLUXES FOR HAEBE STARS

ID	S I 1296 10^{-13}	O I 1304 10^{-13}	Si II 1309 10^{-13}	Si IV 1394 10^{-13}	Si IV 1403 10^{-13}	C IV 1549 10^{-13}	He II 1640 10^{-14}	Si III] 1892 10^{-14}	C III] 1909 10^{-14}
33	4.57 (30)	6.80 (42)	5.49 (30)	6.09 (30)	6.09 (30)	...	...	...	...
37	0.85 (12)	1.92 (23)	0.38 (17)	<0.15	<0.15	0.95 (17)	...	...	...
52	<0.11	0.45 (16)	<0.30	0.12 (04)	0.39 (04)	0.76 (11)	...	2.97 (47)	3.56 (47)
60	0.30 (09)	0.49 (17)	0.53 (12)	0.63 (07)	0.32 (07)	2.79 (22)	5.1 (1.8)	...	...
70	0.26 (11)	0.60 (15)	<0.21	<0.32	<0.36	0.54 (18)	...	...	...
106......	19.8 (1.3)	26.4 (1.8)	24.2 (1.3)	8.1 (1.3)	9.1 (1.3)	18.9 (3.0)	...	...	...
114......	0.44 (11)	0.45 (15)	<0.22	<0.29	<0.30	1.35 (27)	...	...	...
121......	0.93 (29)	3.80 (76)	1.78 (73)	1.89 (16)	1.16 (16)	2.98 (40)	...	...	...
124......	3.54 (40)	10.76 (56)	4.90 (40)	1.28 (40)	1.62 (40)	10.3 (1.1)	...	...	...

NOTE.—Values in each column must be multiplied by the factor at the top of each column. Integrated line fluxes are in units of ergs^{-1} s^{-1} cm^{-2}. Uncertainties in the last two digits are enclosed in parentheses after each value. Tabulated upper limits are twice the measured uncertainty. Absence of a measurement indicates that the line was not apparent in the spectrum.

To define wavelength intervals with and without strong circumstellar absorption features, we divided the co-added spectrum of HD 250550 (strongest absorption in Fig. 7) by the spectrum of HD 100546 (weakest absorption). We then divided this ratio by a low-order polynomial fit through the maxima, empirically removing the effects of differential extinction and normalizing the pseudo-continuum. We smoothed the resulting absorption spectrum with a 3 pixel median filter and identified all spectral segments that were either above or below a residual intensity of 0.85 for at least 5 consecutive pixels. Significant circumstellar absorption is present in the wavelength intervals of 1291–1312, 1323–1337, 1356–1448, 1521–1537, 1542–1587, 1599–1753, 1846–1864 Å, which contain 13, 9, 55, 10, 27, 92, and 11 *IUE* pixels, respectively. There was little or no anomalous absorption in the wavelength intervals of 1277–1290, 1313–1322, 1448–1486, 1492–1520, 1588–1599, 1767–1781, 1789–1845, 1864–1890, and 1896–1922 Å, containing 8, 6, 23, 17, 7, 9, 34, 16, and 16 pixels, respectively. These intervals of regular spectral behavior presumably form predominantly in the stellar photosphere.

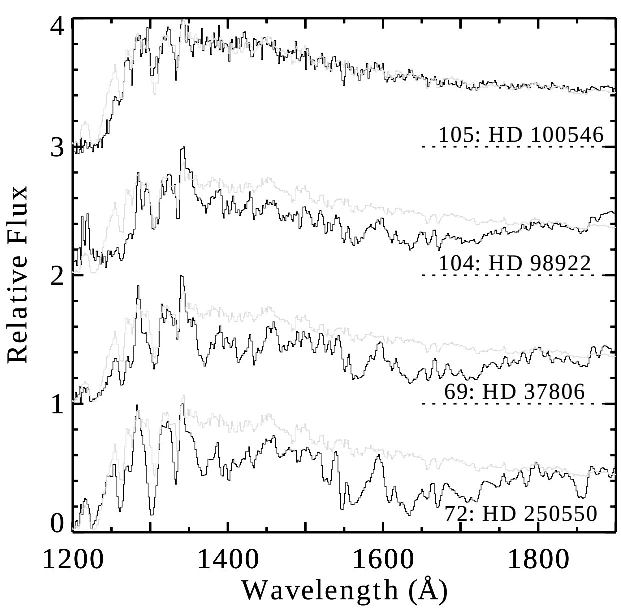

FIG. 7.—HAEBE stars of spectral type B9 with circumstellar absorption line strengths increasing from top to bottom. Dereddened flux spectra in the wavelength range 1200–1900 Å were scaled to yield a peak flux of unity and then offset by integer values. Zero points are indicated by dotted horizontal lines below each star name. Visual extinctions are taken from the Col. (3) of Table 8. For reference, each HAEBE star is compared with a dereddened B9 main sequence star, HD 148579, from Table 9.

To measure circumstellar line depth, an estimate of the underlying photospheric spectrum is required. Ideally, reddened main-sequence templates would provide an accurate proxy of photospheric spectrum, but significant systematic deviations are common. Instead, we resort to a simple empirical estimate of the continuum determined by linearly interpolating the average flux in each of the nine wavelength intervals free of circumstellar absorption. We then divide the observed spectrum by the interpolated continuum in our seven absorbed wavelength intervals, calculating a mean residual. Given the accuracy achievable with these data, we reduce the mean residual intensity to an integer line depth index, D, corresponding roughly to the mean line flux as a fraction of the local continuum in 10% steps. More specifically, $D = 0$, 1, and 2 imply mean line depths 0%–5%, 5%–15%, and 15%–25%, respectively. Larger indexes are defined similarly. A few HAEBE stars show the same lines in emission, rather than absorption, warranting a negative line depth index ($D = -1$, which implies an excess of 5%–15% above the continuum, etc.).

We calculated uncertainties in D by considering contributions from noise in the measured flux spectra and global uncertainty in continuum placement. The impact of noise in the flux spectrum was treated by normal error propagation techniques, whereas the uncertainty in continuum placement was set to half the standard deviation of points about the continuum fitted in the nine continuum windows. This heuristic definition provided the best separation of measurements into detections or 2 σ upper limits. HAEBE stars later than spectral type A4 have so little flux shortward of 1600 Å that we could not reliably measure or even set limits on D. For earlier spectral types, our measured circumstellar line depth indexes or upper limits are given in the last column of Table 8.

Table 8 also gives extinction measurements for most HAEBE stars observed by *IUE*. We determined visual extinction, A_V, by fitting photospheric segments of co-added HAEBE spectra with co-added *IUE* spectra of the main-sequence template stars listed in Table 9. For each spectral subclass in the range B0–A9, we retrieved and co-added all available final archive spectra of the selected tem-

TABLE 8

EXTINCTION FITS TO HERBIG AE/BE STARS

ID[a] (1)	Type (2)	A_V (3)	σ_{A_V} (4)	A_V^{+1} (5)	A_V^{-1} (6)	D[b] (7)
85	B0	1.78	0.01	2.13	...	0
128	B0	1.93	0.28	2.27	...	<7
139	B0	2.67	0.04	3.03	...	<2
54	B1	0.47	0.01	−0.09	0.14	0
49	B1.5	0.66	0.02	0.13	0.78	<2
135	B1.5	2.97	0.05	2.49	3.12	<2
138	B1.5	1.45	0.02	0.87	1.57	<2
83	B2	0.46	0.02	−0.04[c]	1.04	0
88	B2.5	0.80	0.01	0.61	1.34	0
141[d]	B2.5	...	...	...	...	...
154	B2.5	1.59	0.03	1.43	2.08	1
157	B2.5	1.95	0.02	1.77	2.48	0
67	B3	0.14	0.01	0.31	0.43	<2
74	B3	0.31	0.01	0.43	0.55	1
86	B3	−1.00	0.05	−0.83	−0.70	1
156	B3	1.22	0.01	1.38	1.49	0
89	B3.5	1.88	0.01	1.86	2.04	5
55	B4	0.23	0.03	0.08	0.11	<2
2	B5	2.87	0.08	2.80	3.02	3
77	B5	0.63	0.01	0.55	0.84	1
82	B5	1.84	0.02	1.76	2.07	1
84	B5	1.22	0.12	1.16	1.42	4
108	B5	2.13	0.12	2.07	2.33	<3
134	B5	1.88	0.22	1.80	2.07	<5
91	B5.5	0.69	0.01	0.53	0.75	1
81	B6	1.10	0.01	0.78	1.18	2
96	B6	0.74	0.03	0.42	0.81	<2
158	B6	2.03	0.21	1.73	2.06	<4
76	B7	1.01	0.09	1.11	1.38	1
40	B8[e]	0.62	0.02	1.09	0.51	<0[f]
45	B8[e]	1.23	0.02	1.68	1.13	< 2
51	B8	−0.69	0.03	−0.24	−0.77	<2
75	B8	2.20	0.04	2.70	2.05	<2
80	B8	−0.23	0.01	0.22	−0.34	1
66	B8.5	2.94	0.19	2.32	2.56	<5
69	B9	1.88	0.00	−0.56[c]	1.34	3
72	B9	1.35	0.01	−0.99[c]	0.81	3
101	B9	1.84	0.02	−0.50[c]	1.31	<2
104	B9	3.36	0.02	0.94	2.76	1
105	B9	1.03	0.03	−1.11[c]	0.52	<2
109	B9[e]	1.30	0.03	−1.04[c]	0.76	<2
147	B9	1.34	0.01	−0.89[c]	0.84	<2
150	B9.5	2.33	0.03	0.69	3.00	<2
155	B9[e]	1.65	0.14	−0.56	1.09	<3
44	A0	−0.55	0.03	−0.89[c]	1.94	<2
57	A0	0.92	0.06	0.55	3.17	<2
78	A0	0.20	0.16	−0.31	2.29	3
87	A0[e]	−0.04	0.02	−0.62	2.26	2
90	A0	1.65	0.04	1.48	4.24	<2
99	A0	0.24	0.01	−0.06[c]	2.53	<2
136	A0	0.91	0.18	0.26	2.92	−2[f]
145	A0	0.89	0.38	0.49	3.03	...
153	A0	3.56[c]	0.02	2.62[c]	6.06[c]	2
159	A0[e]	0.55	0.03	0.15	2.71	3
31	A1[e]	0.73	0.00	−0.32	1.17	1
63	A1	−0.77	0.02	−1.78	−0.43	2
73	A1[e]	0.27	0.10	−0.59	0.67[c]	<3
142	A1	7.30[c]	0.01	5.44[c]	8.89[c]	2
94	A1.5	−0.13	0.07	−1.71[c]	0.60	2
152	A1.5	1.28	0.06	−0.48	2.14	3
34	A2[e]	0.98	0.04	0.62[c]	2.06	<2
65	A2[e]	0.37	0.08	−0.48[c]	1.28	<4
33	A2.5	8.41[c]	0.06	−1.38[c]	14.08[c]	±2[f]
59	A3[g]	...	...	...	...	<2
106	A4	−1.03	0.02	−1.47[c]	−1.65[c]	<3
148[d]	A5	...	...	...	...	...
70	A7	1.58	0.05	1.88	1.15	...
124	A7	0.21	0.02	0.62	−0.06	...
114	A7.5	1.54	0.08	2.15	1.16	...
36	A8[e]	0.26	0.15	1.25	−0.08	...
37	A8[e]	0.08	0.06	0.99	−0.27	...
52	A8	−0.85	0.22	0.12	−1.25	...
60	A8[e]	−0.11	0.04	0.76	−0.48	...
121	A8.5	−0.03	0.05	0.40	−0.65	...

[a] Identification number from Col. (1) of Table 1.
[b] Mean depth of anomalous absorption relative to the local continuum (in 10% steps, see § 4.2).
[c] Poor template fit; A_V listed for diagnostic purposes only.
[d] Inadequate S/N ratio to allow extinction fit.
[e] Spectral type modified from literature values in Table 1.
[f] Some or all lines in emission.
[g] Spectrum cannot be fitted by a reddened template of any spectral type.

plates, using the co-addition procedure described above for PMS spectra. We then removed the effects of extinction in the co-added template spectra, using the $R = 3.1$ extinction relation of Cardelli, Clayton, & Mathis (1989) and existing measurements of A_V from Neckel, Klare, & Sarcander (1980). Table 9 lists the HD catalog number, adopted spectral type, number of useful *IUE* spectra, and adopted A_V for each template. When A_V in the table is negative, we actually redden the template slightly to achieve a canonical, zero-extinction template. In our bandpass, reddening makes a star peak more strongly, rather than making it redder, because of the influence of a broad absorption feature centered near 2175 Å (Cardelli, Clayton, & Mathis 1989).

We note that A_V is negative for many of our A0–A9 templates. The mean A_V is -0.04 ± 0.03 mag, but this is not necessarily a good test of the zero point since legitimate

TABLE 9

EXTINCTION TEMPLATE STARS

HD	Type	N_{IUE}	A_V[a]
46106	B0 V	3	1.33
144470	B1 V	3	0.75
37776	B2 V	2	0.36
120315	B3 V	48	0.10
136664	B4 V	2	0.08
25340	B5 V	3	0.08
90994	B6 V	3	0.07
87901	B7 V	9	0.08
74604	B8 V	24	0.03
148579	B9 V	3	1.12
172167	A0 V	11	0.01
48915	A1 V	7	−0.02
97633	A2 V	2	−0.16
102647	A3 V	7	0.04
13041	A4 V	2	−0.04
11636	A5 V	10	−0.06
28527	A6 V	1	−0.03
187642	A7 V	4	0.13
28910	A8 V	3	−0.08
180777	A9 V	4	−0.20

[a] Visual extinction from Neckel et al. 1980.

reddening would tend to increase the mean. Neckel et al. (1980) claim A_V uncertainties of 0.1–0.2 mag for individual stars, but there is no particular reason to expect a zero-point error because of their assumed intrinsic $(B-V)$ colors for A stars. Nonetheless, any zero-point error in A_V for our templates will persist in our derived A_V values for HAEBE stars in Table 8.

To determine A_V for each HAEBE star, we extracted relevant template spectra, interpolating as needed to get templates for half-integer subtypes (A9.5, for example). When interpolating, the template spectrum for the later spectral type was first scaled to minimize the absolute value of the difference between the two template spectra. Initially, we adopted literature spectral classes (Table 1) for each HAEBE star, averaging over multiple assignments ("A7/8" becomes A7.5) or adopting median values for incomplete spectral types ("A" becomes A5) as needed. In the course of the extinction analysis, it became clear that some observed HAEBE stars could not be fitted with templates of the assumed spectral class. In these cases, we adopted the nearest spectral class that yielded a plausible fit. The second column of Table 8 gives our adopted spectral classes, indicating by footnote which values have been modified.

We used a nonlinear least-squares analysis to solve for A_V and the global scale factor that best maps a zero-extinction template onto the observed HAEBE star. Only the photospheric windows, relatively free of circumstellar absorption, were used in the fit. We again assumed an $R = 3.1$ extinction law for all HAEBE stars, acknowledging that during episodic extinction enhancements, this value may be inappropriate (Thé et al. 1994). Our derived values of A_V and the corresponding formal uncertainties appear in the third and fourth columns of Table 8. Given the systematic discrepancies in many of the fits, it is likely that these formal errors are negligible compared with systematic errors. As a measure of possible systematic errors, we also have tabulated in Table 8 visual extinctions assuming one spectral subclass earlier (A_V^{+1}) and later (A_V^{+1}) than our adopted spectral class. Derived values of A_V that are much less than zero are retained in the table to indicate the extent to which standard extinction fits fail.

4. DISCUSSION

4.1. H_2 *Emission from CTTS*

Emission lines of H_2 provide a potentially useful constraint on extended gas and radiation in CTTS systems. IR emission lines may be collisionally excited (by shocks or thermal motion) or pumped by UV radiation (Black & van Dishoeck 1987), but H_2 emission in the UV can be caused only by fluorescence. Brown et al. (1981) were the first to detect and identify UV fluorescence of H_2 in an *IUE* spectrum of T Tau. Nearly twenty years later, this is still the only published detection of H_2 emission in the spectrum of a TTS. Despite the implication, we show below that H_2 emission is likely to be common around TTS. In sunspots and near solar flares, Lyα is the most effective fluorescent pumping line (Bartoe et al. 1979). Even at *IUE* resolution, we can discern the by-products of these same pumping routes in spectra of TTS. Higher resolution spectra obtained with *HST* will soon probe the velocity structure of circumstellar H_2 and allow a more detailed exploration of various possible UV pumping mechanisms. Combining UV and IR data may someday yield adequate constraints to formulate a dynamical model of gas within a few stellar radii, which is unresolvable with current imaging technology.

In the 32 CTTS and 5 NTTS where we detected C IV, only 13 CTTS and no NTTS have detectable H_2 emission (see Tables 5 and 6). In Figure 8, we explore the significance of the nondetections by comparing H_2 and C IV line fluxes at Earth. Line fluxes for the two species are correlated, but we have too few H_2 detections to establish whether the relationship is predominantly because of linked line-formation mechanisms or simply because of the distribution of source distances and sizes in our sample. In either case, we can use the correlation and measured C IV line fluxes to explore whether or not some H_2 nondetections imply unusually weak emission. We estimated 2 σ upper limits on H_2 lines by scaling the tabulated C IV uncertainties by 0.77 ± 0.22 based on the behavior of the 12 CTTS in Tables 5 and 6 with uncertainties for both species. Figure 8 shows that most of the stars with H_2 nondetections have such weak C IV that we would not necessarily expect to be able to detect H_2 in *IUE* spectra. The few notable exceptions are AK Sco (No. 133, F5) and perhaps CV Cha (No. 103, G8) and FK Ser (No. 144, K5). AK Sco is the warmest CTTS in our sample, though it is unclear whether this is relevant.

Figure 8 shows fluxes directly from Tables 5 and 6, but as discussed in § 3.3, our "C IV 1549" flux suffers from minor contamination by H_2. Correcting the C IV fluxes by subtracting scaled "H_2 1503" fluxes causes a 10% contraction of the abscissa but has no qualitative effect on the appearance of the figure or its interpretation. In Paper II, we analyze all the TTS emission-line data presented here and explore in detail possible origins for the H_2 emission.

Brown et al. (1981) note that the H_2 emission around T Tau is spatially extended in the raw images obtained by *IUE*. This result is supported by archival *HST* spectra of T

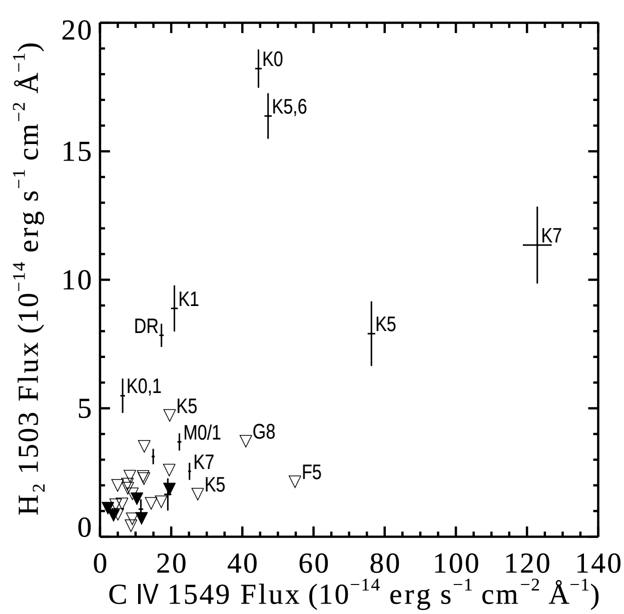

FIG. 8.—Plot of H_2 1503 line fluxes or upper limits vs. C IV 1549 line fluxes. Detections are plotted as orthogonal error bars covering the range ± 1 σ. H_2 upper limits (2 σ) are plotted as downward pointing triangles that are unfilled for CTTS and filled for NTTS. Spectral types are given for sources with relatively large line fluxes. DR Tau (uncertain spectral type) is labeled by name.

Tau obtained with the GHRS. Figure 5 shows a GHRS spectrum of T Tau (data sets Z2DL0407T and Z2DL0409T) convolved with a Gaussian to mimic the 6 Å resolution of *IUE*. Except near O I 1304 Å, the *IUE* spectrum typically has about twice the flux of the GHRS spectrum. This discrepancy is probably not caused by an error in flux calibration. Both data reduction pipelines use the white dwarf G191-B2B as the flux standard, and in fact the GHRS calibration is expected to yield fluxes 6% larger than NEWSIPS (Nichols & Linsky 1996). As indicated in Table 2, the seven *IUE* spectra of T Tau also did not exhibit significant variation. We attribute the greater *IUE* flux to extended emission, primarily but not exclusively in lines of H_2, outside the 1''.74 × 1''.74 aperture of GHRS but inside the 9''.1 × 21''.6 aperture of *IUE*. This interpretation is bolstered by another GHRS spectrum (data sets Z2DL040ET and Z2DL040GT) of T Tau obtained with the 0''.22 × 0''.22 aperture, which has even lower flux levels, especially in fluoresced H_2 lines.

4.2. *Circumstellar Material around HAEBE Stars*

Herbig Ae/Be stars are believed to be intermediate-mass analogs of low-mass TTS, which is our main motivation for including both classes of objects this catalog. Both CTTS and HAEBE stars have excess (nonphotospheric) emission in the near-IR, indicating the presence of dust near the star. In CTTS, accreting gas shocks at the slowly rotating stellar surface, heating to greater than 10^4 K and emitting useful accretion diagnostics (He I emission lines and a UV continuum excess, for example) that can be distinguished from the normal photospheric spectrum. In contrast, HAEBE stars have innate surface temperatures of 10^4 K, making it difficult to distinguish excess accretion luminosity from ordinary stellar emission. This also means that currently there are no direct observations of accretion shock temperatures for HAEBE stars. The kinematic effect of increased stellar mass and more rapid rotation are calculated easily, but we do not yet know the radius at which Keplerian motion in the disk is disrupted, initiating approximate free fall. If there is some modest temperature difference between the photosphere and recently accreted material, it would be most easily detected in the UV, where flux at a given wavelength is a strong function of temperature.

In § 3.4, we measured extinction toward HAEBE stars by fitting low-resolution *IUE* spectra with reddened main-sequence templates, assuming no significant contributions from accretion or other nonphotospheric components. Many of the HAEBE spectra were well fitted by reddened main-sequence templates, but even for these stars we cannot rule out the presence of accreting material at photospheric temperatures. Fits over a broader wavelength range or at higher spectral resolution might yet reveal some hint of accretion. Some of the HAEBE stars in Table 8 were not well fitted or exhibited other peculiarities, inviting further study. We derived negative values of A_V for eight stars and suspiciously low values for several more. These stars are all bluer than is reasonable, suggesting the possible presence of a marginally hotter accretion component. For eight other stars labeled in Table 8, we were able to achieve a decent fit only by adopting a UV spectral type bluer than literature values based on optical spectra. Three HAEBE stars are labeled as having poor template fits, and another three have negative line-depth indexes, thus indicating the presence of emission lines. Finally, the spectrum of T Ori (No. 59) is so unusual that it cannot be fitted by any combination of spectral class and reddening. All of these peculiar stars would be good candidates for further study, though the peculiarities could simply be caused by white dwarf companions or nearby reflection nebulae.

The presence of wind absorption in the spectra of many HAEBE stars certainly has been known and appreciated for years (Catala et al. 1986). Nonetheless, this atlas makes clear the diversity of circumstellar line strengths represented even within narrow spectral type intervals. The last column of Table 8 gives our line-depth index, D, which is defined in § 3.4. The *IUE* spectra presented here are inadequate to resolve and identify individual absorption lines, but a few lines in a few stars have been identified using higher dispersion *IUE* or GHRS spectra. At least some of the circumstellar absorption features in our *IUE* spectra are blueshifted blends of singly ionized atomic resonance lines, suggesting the presence of a massive wind. The absence of these lines in early B-type HAEBE stars may indicate simply that the circumstellar material close to the star is increasingly ionized. In the spectral type interval B5–A4, *none* of the 44 HAEBE stars in our sample has $D = 0$, despite S/N ratios adequate to produce 21 detections of circumstellar absorption. For comparison, six of the 17 early B-type HAEBE stars had $D = 0$, given four detections and seven upper limits. This suggests that massive circumstellar envelopes are quite common throughout the spectral type interval B5–A4. More quantitative statements are not possible without attempting to understand the biases inherent in the set of stars observed by *IUE*. For late A-type HAEBE stars, there is not enough continuum flux at short wavelengths to detect absorption in *IUE* spectra, but near-UV spectra may well reveal the presence of circumstellar absorption by neutral metals.

Many HAEBE stars have excess emission in the IR above that expected for ordinary main-sequence stars with similar spectral types and extinction. This IR excess is attributed to circumstellar dust that is heated either radiatively by the star or via dissipative processes in an accretion disk. Depending on the geometrical distribution of gas and dust near HAEBE stars, there may be a relationship between IR excess and our UV line-depth parameter, D, in Table 8. Hillenbrand et al. (1992) defined three groups of HAEBE stars with progressively more IR excess. Group III had little or no excess, Group I had an excess consistent with a disk, and Group II had the strongest IR excess. We attempted to measure D for 28 HAEBE stars in Hillenbrand et al. (1992); we succeeded for 15, set limits for 10, and failed for 3. Table 10 shows the relationship between D and IR excess. We obtained $D = 0$ for four of the Group III stars and $D < 2$

TABLE 10

LINE-DEPTH DISTRIBUTION

Line Depth	Group III[a]	Group I	Group II
$D = 0$	4	1	0
$D = 1$	0	3	1
$D = 2$	0	1	0
$D = 3$	0	2	1
Emission	0	2	0
Upper Limit	1	8	1
No Value	0	2	1

[a] IR classification from Hillenbrand et al. 1992.

for the remaining star. All of these stars are early B-type stars, so perhaps radiative heating destroys dust, just as it ionizes the gas (see above). In contrast to this orderly result, Table 10 shows a range of possible D values for Group I stars. Both emission-line sources are in this group. Perhaps the diversity of D values reflects a range of disk inclinations, which would affect absorption lines more strongly than IR excess. Finally, our Group II stars have $D = 1$ and 3, plus an upper limit. This could be construed as evidence for large circumstellar absorption in Group II stars, which might be sensible, but in fact the results are statistically equivalent to the distribution of D values for Group I stars.

4.3. *Future Work*

We have attempted here to compile a fairly complete survey of available *IUE* data to serve as a guide for future investigations of PMS stars. In Paper II, we compare the TTS line fluxes in Tables 5 and 6 with line fluxes for main-sequence and evolved stars as a function of stellar parameters relevant to magnetic dynamos. We conclude that most of the UV emission from CTTS is generated by accretion rather than magnetic activity. Goméz de Castro & Franqueira (1997b) provide an example of how *IUE* time series data can be used to study both magnetic activity and accretion in CTTS. Table 2 indicates TTS and HAEBE stars that varied significantly between observations with *IUE*, making these promising candidates for future temporal studies. *HST* now provides improved UV sensitivity and spectral resolution. Investigations at high spectral resolution will be especially useful for measuring the kinematics of TTS emission lines and HAEBE circumstellar absorption features, thus providing new constraints on accretion models. Higher spectral resolution will also make it possible to achieve a detailed understanding of the molecular hydrogen fluorescence routes operating in CTTS. Targets for all of these projects will likely be selected on the basis of the initial survey provided by *IUE*.

We thank the *IUE* final archive team for providing an extremely valuable resource to the community. We also thank Wayne Landsman for maintaining the IDL software libraries and databases we used when selecting our sample and finding associated *IUE* spectra. In addition, this research has made use of the SIMBAD database, operated at CDS, Strasbourg, France. Finally, we thank Marc Gagné, Alexander Brown, Michael Meyer, and Lynn Hillenbrand for helpful discussions.

REFERENCES

Abgrall, H., Roueff, E., Launay, F., Roncin, J.-Y., & Subtil, J.-L. 1993, A&AS, 101, 273
Appenzeller, I., & Mundt, R. 1989, A&A Rev., 1, 291
Bartoe, J.-D. F., Brueckner, G. E., Nicolas, K. R., Sandlin, G. D., Vanhoosier, M. E., & Jordan, C. 1979, MNRAS, 187, 463
Basri, G., & Bertout, C. 1993, in Protostars and Planets III, ed. E. H. Levy & J. I. Lunine (Tucson: Univ. of Arizona Press), 543
Bertout, C. 1989, ARA&A, 27, 351
Black, J. H., & van Dishoeck, E. F. 1987, ApJ, 322, 412
Blanco, A., Fonti, S., & Strafella, F. 1988, A&A, 197, 249
Blondel, P. F. C., Talavera, A., & Djie, H. R. E. T. A. 1993, A&A, 268, 624
Blondel, P. F. C., & Tjin a Djie, H. R. E. 1994, in ASP Conf. Proc., 62, The Nature and Evolutionary Status of Herbig Ae/Be Stars (San Francisco: ASP), 211
Boehm, T., et al. 1996, A&AS, 120, 431
Böhm, T., & Catala, C. 1993, A&AS, 101, 629
———. 1994, A&A, 290, 167
Bouret, J.-C., & Catala, C. 1998, A&A, 340, 163
Bouret, J.-C., Catala, C., & Simon, T. 1997, A&A, 328, 606
Brown, A., Jordan, C., Millar, T. J., Gondhalekar, P., & Wilson, R. 1981, Nature, 290, 34
Cardelli, J. A., Clayton, G. C., & Mathis, J. S. 1989, ApJ, 345, 245
Catala, C., Czarny, J., Felenbok, P., & Praderie, F. 1986, A&A, 154, 103
De Winter, D., Grady, C. A., Van den Anckner, M. E., Pérez, M. R., & Eiroa, C. 1999, A&A, 343, 137
Feigelson, E. D., Casanova, S., Montmerle, T., & Guibert, J. 1993, ApJ, 416, 623
Ghandour, L., Strom, S. E., Edwards, S., & Hillenbrand, L. A. 1994, in ASP Conf. Proc., 62, The Nature and Evolutionary Status of Herbig Ae/Be Stars (San Francisco: ASP), 223
Giampapa, M. S., Calvet, N., Imhoff, C. L., & Kuhi, L. V. 1981, ApJ, 251, 113
Goméz de Castro, A. I., & Franqueira, M. 1997a, *International Ultraviolet Explorer*—Uniform Low Dispersion Archive T Tauri Stars, *IUE*—ULDA Access Guide No. 8 (Paris: ESA)
———. 1997b, ApJ, 482, 465
Goméz de Castro, A. I., & Lamzin, S. A. 1999, MNRAS, 304, L41
Grady, C. A., Perez, M. R., Bjorkman, K. S., & Massa, D. 1999a, ApJ, 511, 925
Grady, C. A., Sitko, M. L., Bjorkman, K. S., Perez, M. R., Lynch, D. K., & Russell, R. W. 1997, ApJ, 483, 449
Grady, C. A., Woodgate, B., Bruhweiler, F. C., Boggess, A., Plait, P., & Lindler, D. J. 1999b, ApJ, 523, L151
Hartmann, L., & Kenyon, S. 1996, ARA&A, 34, 207
Hartmann, L., Kenyon, S. J., & Calvet, N. 1993, ApJ, 407, 219
Herbig, G. H., & Bell, K. R. 1988, Third Catalog of Emission-Line Stars of the Orion Population, Lick Obs. Bull. No. 1111
Herbig, G. H., & Goodrich, R. W. 1986, ApJ, 309, 294
Hillenbrand, L. A., Strom, S. E., Vrba, F. J., & Keene, J. 1992, ApJ, 397, 613
Huélamo, N., Franqueira, M., & Goméz de Castro, A. I. 2000, MNRAS, 312, 833
Imhoff, C. L., & Appenzeller, I. 1987, Exploring the Universe with the *IUE* Satellite, ed. Y. Kondo (Dordrecht: Reidel), 295
Johns-Krull, C. M., Valenti, J. A., & Linsky, J. L. 2000, ApJ, 539, 815 (Paper II)
Jones, B. F., & Walker, M. F. 1988, AJ, 95, 1755
Landsman, W., & Simon, T. 1993, ApJ, 408, 305
Malfait, K., Bogaert, E., & Waelkens, C. 1998, A&A, 331, 211
Neckel Th., Klare G., & Sarcander M. 1980, A&AS, 42, 251
Nichols, J. S., Garhart, M. P., De La Peña, M. D., & Levay, K. 1994, NASA *IUE* Newsl. No. 53
Nichols, J. S., & Linsky, J. L. 1996, AJ, 111, 517
Praderie, F., Catala, C., Simon, T., & Boesgaard, A. 1986, ApJ, 303, 311
Rodríguez-Pascual, P. M., González-Riestra, R., Schartel, N., & Wamsteker, W. 1999, A&AS, 139, 183
Sandlin, G. D., Bartoe, J.-D. F., Brueckner, G. E., Tousey, R., & VanHoosier, M. E. 1986, ApJS, 61, 801
Shu, F. H., Adams, F. C., & Lizano, S. 1987, ARA&A, 25, 23
Simon, T., Vrba, F. J., & Herbst, W. 1990, AJ, 100, 1957
Thé, P. S., de Winter, D., & Pérez, M. R. 1994, A&AS, 104, 315
Walter, F. M. 1987, PASP, 99, 31
Walter, F. M., Vrba, F. J., Mathieu, R. D., Brown, A., & Myers, P. C. 1994, AJ, 107, 692
Waters, L. B. F. M., & Waelkens, C. 1998, ARA&A, 36, 233